Available online at www.sciencedirect.com

ScienceDirect

International Journal of Solids and Structures 45 (2008) 2420–2450

INTERNATIONAL JOURNAL OF SOLIDS AND STRUCTURES

www.elsevier.com/locate/ijsolstr

Mechano-sorptive creep under compressive loading – A micromechanical model

Jessica Strömbro, Peter Gudmundson *

KTH Solid Mechanics, Royal Institute of Technology, SE-100 44 Stockholm, Sweden

Received 28 June 2007; received in revised form 19 November 2007
Available online 14 December 2007

Abstract

The creep of paper is accelerated by moisture cycling, an effect known as mechano-sorptive creep. It has also been observed that the mechano-sorptive effects are larger in compression than in tension. In this paper a simplified network model for mechano-sorptive creep is presented. It is assumed that the anisotropic hygroexpansion of the fibres leads to large stresses at the fibre–fibre bonds when the moisture content changes. The resulting stress state will accelerate creep if the fibre material obeys constitutive laws that are non-linear in stress. Geometrical fibre effects are included in the model in order to capture experimental observations of the differences between paper loaded in tension and compression. Theoretical predictions based on the developed model are compared to experimental results for paper both under tensile and compressive loading at varying moisture content. The important features in the experiments are captured by the model, i.e. the creep is accelerated by the moisture cycling and the mechano-sorptive effects are larger in compression than in tension.

Keywords: Mechano-sorptive creep; Accelerated creep; Paper; Modelling; Moisture changes; Humidity change; Sorption; Fibres; Creep; Network model; Fibre network; Mathematical model; Fibre bonding; Tension; Compression

1. Introduction

Packages of paper often have to withstand loads for long times, and therefore is creep, i.e. time dependent deformation, an important factor in package design. The creep is affected by humidity conditions. High humidity, and therefore high moisture content in the paper, means faster creep compared to low humidity (Brezinski, 1956; Söremark and Fellers, 1993; Söremark et al., 1993; Haslach, 1994). Moreover, creep is accelerated by varying humidity, so that the creep during cycling between low and high humidity is likely to exceed the creep at constant humidity even at the highest level, a phenomenon known as mechano-sorptive creep or accelerated creep (Byrd, 1972a,b; Söremark and Fellers, 1993; Söremark et al., 1993; Haslach, 1994; Habeger and Coffin, 2000). This makes it difficult to predict deformation and life-time of packages stored under varying humidity conditions.

* Corresponding author. Tel.: +46 8 790 75 48; fax: +46 8 411 24 18.
E-mail address: peter@hallf.kth.se (P. Gudmundson).

0020-7683/$ - see front matter
doi:10.1016/j.ijsolstr.2007.12.002

Mechano-sorptive creep was independently discovered for wool (Mackay and Downes, 1959; Nordon, 1962) and wood (Armstrong and Kingston, 1960; Armstrong and Christensen, 1961) in late 1950s and early 1960s. In 1972, Byrd (1972a,b) found experimental evidence for accelerated creep in paper. A similar behaviour has also been found in concrete (Pickett, 1942) and in the 1990s mechano-sorptive creep was found in some synthetic fibres, for example aramid (Kevlar) fibres (Wang et al., 1990, 1992, 1993), and in Kevlar fibre reinforced epoxy composites (Wang et al., 1990). A common property of these materials is that they contain hydrogen bonds.

There is no generally accepted model for mechano-sorptive creep. Several ideas of the physical mechanism of mechano-sorptive creep have been presented. It has for example been suggested that during moisture content changes a non-equilibrium state occurs, in which hydrogen bonds will be broken and recreated by the interaction with migrating water molecules (Gibson, 1965). It has also been suggested that moisture content changes generate free volume in the material, i.e. the volume available for molecular movements increases, which would lead to an increase in creep compliance (Padanyi, 1991, 1993). Other models explain the mechano-sorptive effect by dislocations, for example kinks and slip planes, which are created and affected by stresses caused by moisture content changes. Compressive loading would lead to an increased number of dislocations and more dislocations lead to a higher hygroexpansion and lower stiffness (Hoffmeyer and Davidson, 1989; Hoffmeyer, 1993; Söremark and Fellers, 1993). A model combining these mechanisms, i.e. creation of free volume, bond breaking and formation of dislocations, has also been proposed (Haslach, 1994). Experiments using IR-spectra indicated that additional creep mechanisms on a molecular level are activated during moisture cycling compared to constant moisture (Olsson and Salmén, 2001). Phenomenological models that do not take actual micro-mechanisms into account have also been presented. Ranta-Maunus (1975) developed a generalized viscoelastic model for wood that includes moisture changes. Later Mårtensson (1994) followed Ranta-Maunus idea and developed an incremental strain–stress relationship for wood. Urbanik (1995) suggested a model for corrugated boards subjected to a constant compression load and humidity cycling. In this model the total deformation is the sum of the hygroexpansion and the mechano-sorptive creep.

In some recent investigations (Habeger and Coffin, 2000; Alfthan et al., 2002; Alfthan, 2003, 2004; Alfthan and Gudmundson, 2005) it has been suggested that mechano-sorptive creep in paper is an effect of non-linear creep of the individual fibres in combination with large transient stresses created during moisture content changes which give rise to redistribution of stresses. There are also other scientists that have proposed that stress redistribution is of importance (Armstrong and Christensen, 1961; Söremark and Fellers, 1993), but this model is basically a further development of Pickett's ideas from 1942. The principal controlling mechanism for accelerated creep in paper at varying moisture contents is the hygroscopic nature and the anisotropic properties of the individual fibres in combination with their non-linear creep behaviour. One particular kind of material heterogeneity in paper is the difference in hygroexpansion along and across the fibres. The fibre swelling and shrinkage due to moisture content changes are much larger transverse to the fibre axis in comparison to the axial direction of the fibres (Gallay, 1973). Also the mechanical properties, like stiffness, differ quite significantly between the transverse and axial direction of the fibres (Schulgasser and Page, 1988; Bergander and Salmén, 2002; Salmén, 2004). When moisture is changed, the fibres will expand (or shrink). At the bonds, the expansion is restricted by the crossing fibres because of the anisotropic hygroexpansive properties. Instead large stresses are created. In resemblance with the material heterogeneities, moisture gradients also cause heterogeneous hygroexpansive strains, which introduce similar internal stresses because of the restriction by the surrounding material. The internal stresses will be added to the stress state caused by external mechanical loads (van den Akker, 1962). This stress redistribution gives rise to an increased creep rate, driven by the non-linear creep of the fibres. The stresses in the network relax with time during creep and the internal stress state will even out. After a while a new change in moisture content is required to create a new redistribution of stresses and to further accelerate the creep. The advantage of this kind of model is that accelerated creep turns out to be a natural consequence of regular creep, and not a completely new phenomenon.

The most important load cases in packages are compression and bending. There are many experimental observations that indicate a different behaviour in compression in comparison to tension (Byrd, 1972a,b; Söremark and Fellers, 1993; Söremark et al., 1993). Examples are:

- The mechano-sorptive effects are larger in compression than in tension.

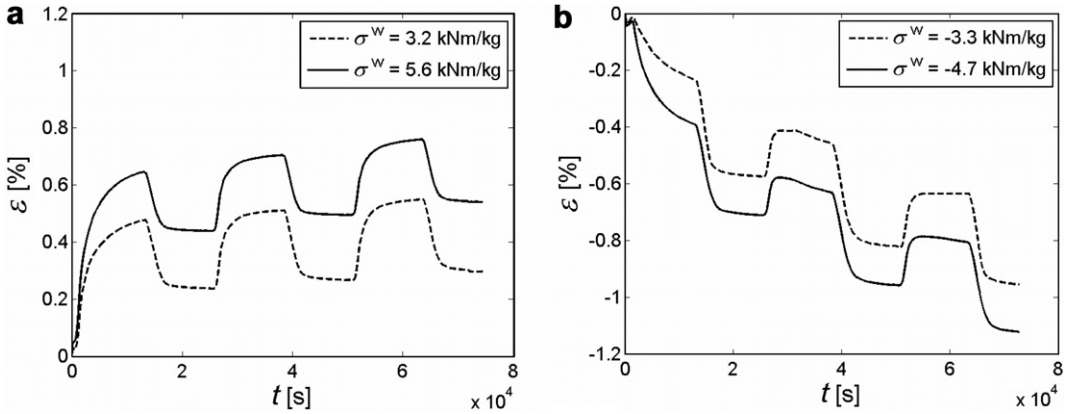

Fig. 1. Mechano-sorptive creep of kraft paper in tension (a) and compression (b). Results from experiments (done by STFI-Packforsk), presented as strain vs. time for cyclic relative humidity (50–90% RH) at different specific stress levels.

- The modulus of elasticity of paper is altered by mechano-sorptive creep, it decreases under mechano-sorptive creep in compression and it increases in tension.
- The moisture expansion coefficient is lower and the modulus of elasticity is higher for a paper that has been subjected to constrained drying compared to a paper that has been subjected to free drying.

In Fig. 1 mechano-sorptive creep is shown from experiments on kraft paper produced at STFI-Packforsk which was dried under restraint and has a grammage of 100 g/m^2 and a thickness of 0.121 mm, in both tensile and compressive loading. It can be observed that the paper creeps faster in compression, which leads to more deformation at a given time and stress level.

The differences between tensile and compressive behaviour are probably an effect of the geometrical fibre properties, e.g. fibre curl and kinks. As pointed out earlier in this section, the moisture expansion in the transverse direction of a fibre is much larger than that in the longitudinal direction. If an initially curved fibre is considered, an increase in moisture content will then decrease the curvature, this will also be the effect if a tensile load is applied, while the curvature will increase with increasing compressive load. This has a consequence that the stiffness will decrease with increased compressive loading, and vice versa, since the fibre compliance increase with the curvature. The effects of fibre geometry such as curvature has so far been neglected in the network modelling of mechano-sorptive creep, but in order to develop a model that accurately can capture mechano-sorptive creep both under tension and compression, and the differences between these two load cases, geometrical effects must be considered. Such a model should also be able to capture the mechano-sorptive behaviour in bending, since bending induces compression and tensile strains in the paper (Söremark and Fellers, 1993; Söremark et al., 1993).

In the present work, a simplified network model is used to study mechano-sorptive creep in paper. Geometrical fibre effects are included to capture experimental observations for paper loaded in both tension and compression. The micromechanical model is presented in Section 2. A single kinked fibre is first considered. The fibre model is then used to develop a fibre-network model. Thereafter, the numerical evaluation of the network model is discussed. In Section 3, the experimental work is described. In order to apply the model a number of material parameters has to be determined, which is done in Section 4. In Section 5, theoretical predictions based on the developed model are compared to experimental results for paper both under tensile and compressive loading at varying moisture content. Finally, in Section 6 conclusions are drawn.

2. Micromechanical model

2.1. The fibre model

In the present paragraph a model for the constitutive relationship between the force and displacement that act between the ends of a free fibre segment will be derived. Instead of forces and displacements, correspond-

ing stresses and strains will be considered. The so derived model will in subsequent paragraphs be applied in a fibre network model.

In order to develop a micromechanical model that accurately can capture the mechano-sorptive behaviour, both in tension and compression, the effects of fibre geometry such as curvature and kinks must be considered. As an approximation, the free fibre segments between fibre–fibre bonds are modelled as two straight bars that form an angle θ. Bending deformations in the bars and in the kink are approximately captured by a non-linear torsional spring, as shown in Fig. 2. It is assumed that all bending deformation is collected in the kink. Hence, in the subsequent analysis the bending deformation in the bars will be neglected.

In the following analysis it will be assumed that the kink angle θ is moderate in the sense that terms of order θ^2 will be of the same order as normal strains in the bars $\varepsilon \ll 1$. This type of approximation is analogous to models for bending of axially loaded beams or models for bending of membrane loaded plates (von Karman theory).

The equilibrium equation for a bar is given by

$$\sigma A l \frac{\theta}{2} + M = 0, \tag{1}$$

where σ is the normal stress in the bar, A is the cross section area, l is the length, M is the moment by the spring and θ is the kink angle, see Fig. 3.

The axial displacement u consists of two parts, the elongation of the bars, u_1, and the displacement u_2 caused by changes in the kink angle θ. This can also be expressed in terms of strains

$$\varepsilon = \varepsilon_1 + \varepsilon_2. \tag{2}$$

It is assumed that the normal strain of the bars, ε_1, can be divided into three parts,

$$\varepsilon_1 = \varepsilon_e + \varepsilon_\beta + \varepsilon_c, \tag{3}$$

where ε_e is the elastic strain, ε_β is the hygroexpansive strain and ε_c is the creep strain. As a consequence of this assumption it is supposed that the superposition of hygroexpansion and creep strain is valid on the fibre level. The elastic and hygroexpansive strains are assumed to be linear functions of stresses and moisture content, respectively,

$$\varepsilon_e = \frac{\sigma}{E_L} \tag{4}$$

and

$$\varepsilon_\beta = \beta_L \Delta m, \tag{5}$$

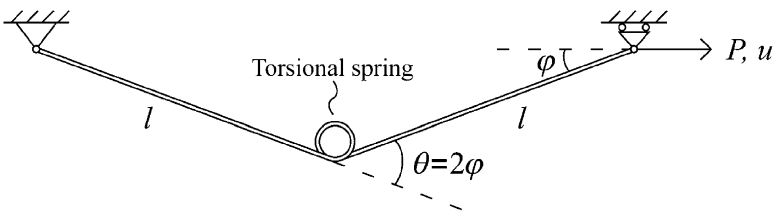

Fig. 2. The fibre model.

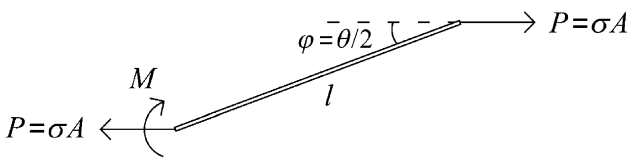

Fig. 3. One of the bars in the fibre model with applied and reaction forces and moment.

where E_L is the modulus of elasticity in the axial direction of the fibre, β_L is the hygroexpansion coefficient along the fibre and Δm is the moisture content change relative a reference level. The creep strain is given by a creep law. Unfortunately, generally accepted creep laws are available neither for paper nor for pulp fibres. Here the following creep law is used

$$\dot{\varepsilon}_c = a \sinh(b(\sigma - E_c \varepsilon_c)), \tag{6}$$

where a, b and E_c are material parameters. This model is based on Eyring's molecular model (Halsey et al., 1945; Holland et al., 1946; Sedlachek, 1995) which represents the rheological behaviour of fibres by applying the kinetic theory of rate processes to the relative movement of flow units in the fibre. The Eyring model can be represented by a combination of two Hookean springs and a nonlinear dashpot element. The dashpot behaviour is represented by a hyperbolic sine law of viscous flow. Eyring proposed that the dashpot represents the flow of the cellulosic chain units. Based on this theory the material parameters a, b and E_c have physical meanings. The parameter a has the dimensional unit s^{-1} and it contains the effects of the modulus of elasticity for the linear chain molecular and the molecular network, the temperature, the free energy of activation for the flow process, the volume of the flowing cellulose and the volume of the voids/empty spaces within the polymeric material/fibre. The parameter b has the dimensional unit Pa^{-1} and contains the effects of the modulus of elasticity for the linear chain molecular and the molecular network, the temperature and the volume of the voids/empty spaces within the polymeric material/fibre. The parameter E_c has the dimensional unit Pa and contains the effects of the modulus of elasticity for the linear chain molecular and the molecular network. A decelerating creep rate is captured by this creep law, which will give a creep response resembling those of paper and fibres (Brezinski, 1956; Söremark and Fellers, 1993; Söremark et al., 1993; Haslach, 1994; Sedlachek, 1995; Olsson and Salmén, 2001). Written in a slightly different form, this kind of creep law has been used to model creep of single fibres (Sedlachek, 1995). One characteristic of this creep law is that the driving force for the creep, $b(\sigma - E_c\varepsilon_c)$, also will decrease as creep takes place, eventually leading to a linear behaviour. If $b(\sigma - E_c\varepsilon_c)$ becomes zero the creep will stop, i.e. there is an ultimate creep limit $\varepsilon_c = \sigma/E_c$. The creep rate of the model seems to decrease too fast compared to experimental data (Sedlachek, 1995), although a long-term equilibrium behaviour is reasonable for polymeric materials (Haslach and Zeng, 1999).

The strain caused by the curvature change, ε_2, can be derived from a geometrical consideration,

$$\varepsilon_2 = \cos\left(\frac{\theta}{2}\right) - \cos\left(\frac{\theta_0}{2}\right) \approx \frac{1}{8}\left(\theta_0^2 - \theta^2\right), \tag{7}$$

where θ_0 is the initial kink angle. In the Taylor expansion of the cosine functions, terms up to second order are considered in accordance with the assumption of moderate kink angles as was discussed above. The kink angle θ is assumed to consist of several parts, the initial angle θ_0, an elastic part θ_e, a hygroexpansive part θ_β and also a creep contribution θ_c, i.e.

$$\theta = \theta_0 + \theta_e + \theta_\beta + \theta_c. \tag{8}$$

The elastic angle change is assumed to be linearly dependent on the torsional spring moment M according to Figs. 2 and 3,

$$\theta_e = \frac{M}{k}, \tag{9}$$

where k is a torsional spring constant. The torsional spring moment can be eliminated by use of Eq. (1),

$$\theta_e = -\frac{\sigma A l}{2k}\theta. \tag{10}$$

In Appendix A1 the torsional spring constant is estimated from beam theory, see Eq. (A5),

$$k = q_k \frac{EI}{l}, \tag{11}$$

where q_k is a non-dimensional constant and I is the moment of inertia of the fibre cross section. The hygroexpansive angle change is assumed to be linearly dependent on the moisture content change

$$\theta_\beta = \beta_m \Delta m, \tag{12}$$

where β_m is the hygroexpansion coefficient for the kink angle. In Appendix A2, β_m is estimated from the hygroexpansion coefficients for the fibre, along and transverse to the fibre axis, see Eq. (A17),

$$\beta_m = -(\beta_T - \beta_L) \cdot (\theta_0 + \theta_c). \tag{13}$$

As can be seen, the hygroexpansive angle change θ_β is assumed to depend on the initial angle, θ_0, and also on the creep angle, θ_c, through the hygroexpansion coefficient β_m. As an approximation the hygroexpansion coefficient is assumed to depend only on the permanent deformations and not the elastic part, θ_e.

The change in kink caused by creep in the spring is given by the creep law

$$\dot{\theta}_c = K_1 \sinh(K_2(M - K_3\theta_c)), \tag{14}$$

where K_1, K_2 and K_3 are material parameters. This is the same type of creep law as for the creep strain in the bars, compare with Eq. (6). If the moment in Eq. (14) is eliminated by use of Eq. (1) the equation will read

$$\dot{\theta}_c = -K_1 \sinh\left(K_2\left(\frac{Al}{2}\sigma\theta + K_3\theta_c\right)\right). \tag{15}$$

In Appendix A3, the constants K_1, K_2, K_3 are estimated, see Eqs. (A26), (A27) and (A28), as

$$K_1 = k_1 \frac{al}{H}, \tag{16}$$

$$K_2 = k_2 \frac{b}{BH^2}, \tag{17}$$

$$K_3 = k_3 \frac{E_c BH^3}{l}, \tag{18}$$

where a, b and E_c are constants in the creep law for the strain in the bars given by Eq. (6), B is the width of the bars and H is the height, k_1, k_2, k_3 are non-dimensional constants. Here it has been assumed that the fibres have a rectangular cross section.

The fibre model presented above defines a constitutive relationship between normal stress σ and effective strain ε of a kinked fibre according to Fig. 2. If the normal stress σ is known as a function of time, the resulting strain $\varepsilon(t)$ can be calculated and vice versa, provided that all material parameters are known. In the next paragraph a network of kinked fibre segments will be considered and the macroscopic paper properties will be derived by a homogenization procedure.

This fibre model captures some important features. The moisture expansion in the transverse direction of a fibre is much larger than that in the longitudinal direction. As is observed in Eqs. (12) and (13), an increase in moisture content will then have as an effect that the curvature of an initially curved fibre will decrease. Also, the curvature of an initially curved fibre will increase with increasing compressive load. Vice versa, the curvature will decrease for tensile loading.

2.2. The network model

The network model presented here is based on the work by Alfthan (2003), but with a more advanced fibre model. Alfthan's network model resembles the network model by Cox from 1952, which was a first attempt to model the influence of fibres on sheet properties. Cox's model only considered elastic behaviour while Alfthan's model added creep, hygroexpansion and the influence of bonds.

In a fibre network each fibre is bonded to many other fibres. The free fibre segments between the fibre bonds are modelled using the fibre model described in Section 2.1, see Figs. 2 and 4. In the network model the fibres consist of free segments, section A, and bonded areas, section B, see Figs. 4 and 5. The length of the free fibre segment is denoted L_f and the total length of the segment is denoted L, see Fig. 5. There is also one more section that is of interest, this is the bonded area of the crossing fibres, section C, see Fig. 4. The model does not include any effects of the finite length of fibres in real paper, i.e. the fibres are assumed to be long, well-bonded fibres. It is also assumed that each fibre–fibre bond only involves two fibres. In addition all fibres segments and

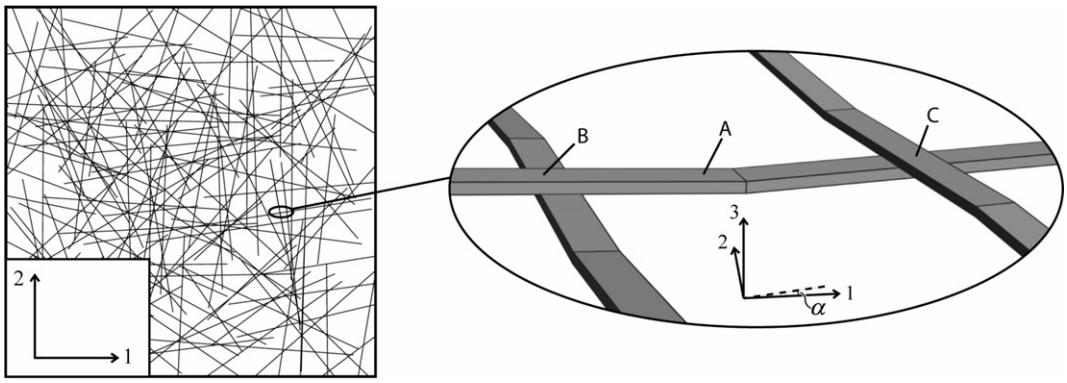

Fig. 4. The fibre network. Each fibre is bonded to many other fibres. For each fibre segment the fibre model is used. A, B and C denotes the different fibre parts.

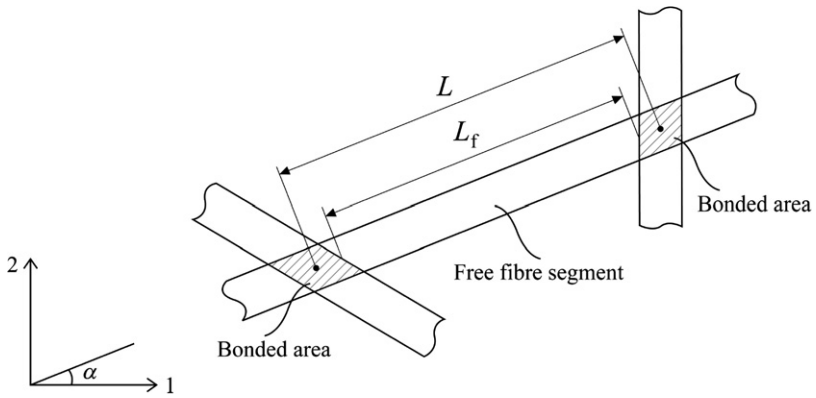

Fig. 5. The geometry of a fibre segment. The direction of the fibre is defined by the angle α measured from the 1-axis of the coordinate system.

fibres bonds are considered equal. In the model, the fibres carry a load in the longitudinal direction only, i.e. only axial stresses appear in the free fibre segments. In a real paper, the length of the free segments between the bonds may be small compared to the width of the fibres and other stress components than axial stresses may therefore arise. In the model it is also approximated that the stresses are uniform at the bonds and shear stresses are not taken into account. It is however believed that the main characteristics of mechano-sorptive creep will be captured by the considered simplified model.

From experiments done by Page and Tydeman (1962) on paper it has been found that there is no relative movement of the fibres at their crossings when the sheet is deformed, so both the bonded and the free segments deform, and the mean strain of a fibre segment is equal to the mean fibre strain. It is also found that the longitudinal strain of a fibre is the same as the strain of the sheet. When the fibre shrinks it is believed that much of the deformation in the free segments is caused by kinks. Another important mechanism is microcompressions in the fibre–fibre bonds, but this has not been included in the present model. It has also been found that the fibre–fibre bonds are sufficiently strong, so that the transverse deformation of a crossing fibre influences the fibre and its longitudinal deformation. DeMaio and Patterson (2006) have performed experiments on paper with different bond strengths between the fibres. The results showed that, as long as there is a sufficient bonding between the fibres, additional increase of the bonding strength does not influence constant humidity creep or mechano-sorptive creep. However, bonds are believed to be necessary for mechano-sorptive creep since individual fibres do not seem to exhibit an accelerated creep behaviour (Sedlachek, 1995). Recently experiments by Olsson et al. (2007) have however indicated that mechano-sorptive creep behaviour also may be present in single wood fibres. All the above observations support the ideas and approximations in

the network model. DeMaio and Patterson's interpretation of their experimental results (2006) was that they agreed with the argument that the mechanisms behind constant creep and mechano-sorptive creep are the same, as is assumed in this work and also, for example, in the works by Habeger and Coffin (2000) and Alfthan et al. (2002, 2003, 2004, 2005). Although some other researchers, for example Gibson (1965), Padanyi (1991, 1993), Hoffeyer and Davidson (1989, 1993), believed that there are different mechanisms behind the constant creep and mechano-sorptive creep.

It is assumed that the normal strain ε of each fibre is determined from the macroscopic strains $\bar{\varepsilon}_{11}, \bar{\varepsilon}_{22}$ and $\bar{\varepsilon}_{12}$, where 1 and 2 denotes the coordinate direction in the plane of the paper and the bar indicates a macroscopic quantity. The average strain of a fibre ε, which also corresponds to the average strain in a fibre segment, is given by

$$\varepsilon = \bar{\varepsilon}_{11}\cos^2\alpha + \bar{\varepsilon}_{22}\sin^2\alpha + 2\bar{\varepsilon}_{12}\cos\alpha\sin\alpha, \tag{19}$$

where α is the angle of the fibre with respect to the 1-axis, see Fig. 5. If the strain of the free segments of a fibre is ε_A and the strain of the bonded length is ε_B, then the average strain of the fibre will be

$$\varepsilon = \frac{L_f}{L}\varepsilon_A + \frac{L - L_f}{L}\varepsilon_B = \lambda\varepsilon_A + (1-\lambda)\varepsilon_B, \tag{20}$$

where $\lambda = L_f/L$.

Since a perfect bonding is assumed, the transverse strain of the crossing fibres, ε_C, will be the same as the strain of the bonded length, ε_B, i.e.

$$\varepsilon_C = \varepsilon_B. \tag{21}$$

If the load carrying area of a crossing fibre is equal to the cross-sectional area of the fibre, the stress in the free segments of a fibre will be the sum of the stresses in the fibres at the bonds,

$$\sigma_A = \sigma_B + \sigma_C, \tag{22}$$

where σ_A and σ_B are the stresses in the axial direction of the fibre in the free segments and at the bonds, respectively, and σ_C is the transverse stress in the crossing fibre, as shown in Fig. 6.

The macroscopic specific stresses in the paper, $\bar{\sigma}^w_{11}, \bar{\sigma}^w_{22}$ and $\bar{\sigma}^w_{12}$, i.e. the stresses divided by the paper density, are equal to the volume average fibre stresses divided by paper density,

$$\bar{\sigma}^w_{11} = \frac{1}{\rho_p}V_f\int_0^\pi \sigma_A f(\alpha)\cos^2\alpha \mathrm{d}\alpha = \frac{1}{\rho_f}\int_0^\pi \sigma_A f(\alpha)\cos^2\alpha\ \mathrm{d}\alpha, \tag{23}$$

$$\bar{\sigma}^w_{22} = \frac{1}{\rho_p}V_f\int_0^\pi \sigma_A f(\alpha)\sin^2\alpha \mathrm{d}\alpha = \frac{1}{\rho_f}\int_0^\pi \sigma_A f(\alpha)\sin^2\alpha\ \mathrm{d}\alpha, \tag{24}$$

$$\bar{\sigma}^w_{12} = \frac{1}{\rho_p}V_f\int_0^\pi \sigma_A f(\alpha)\cos\alpha\sin\alpha \mathrm{d}\alpha = \frac{1}{\rho_f}\int_0^\pi \sigma_A f(\alpha)\cos\alpha\sin\alpha\ \mathrm{d}\alpha, \tag{25}$$

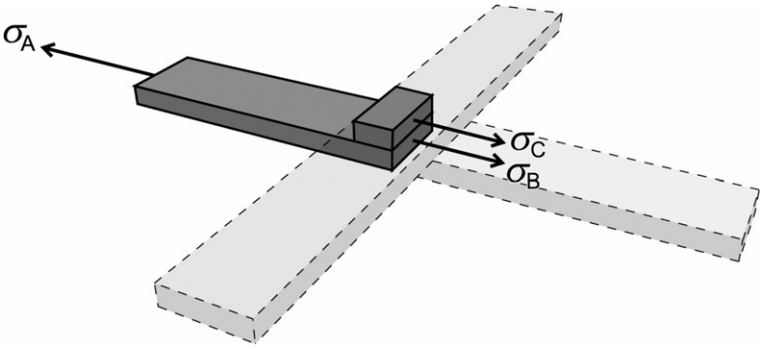

Fig. 6. Definition of the stresses σ_A, σ_B and σ_C.

where ρ_p is the paper density given by $\rho_p = V_f\rho_f$, V_f is the volume fraction of fibres, ρ_f is the fibre density and $f(\alpha)$ is the frequency function for the fibre angle distribution. The frequency function must fulfil the condition

$$\int_0^\pi f(\alpha)\mathrm{d}\alpha = 1. \tag{26}$$

In the subsequent analysis it is assumed that the fibres are uniformly distributed in all directions, i.e. $f(\alpha) = 1/\pi$, corresponding to an isotropic behaviour.

The strain on the fibre level in sections B and C are assumed to be the sum of elastic, hygroexpansive and creep strains. To simplify, it is assumed that all fibre crossings are perpendicular. The elastic and hygroexpansive strains are assumed to be linear functions of stresses and moisture content, respectively. The strain in section B and C then becomes

$$\varepsilon_B = \varepsilon_B^e + \varepsilon_B^h + \varepsilon_B^c = \frac{\sigma_B}{E_L} + \beta_L\Delta m + \varepsilon_B^c, \tag{27}$$

$$\varepsilon_C = \varepsilon_C^e + \varepsilon_C^h + \varepsilon_C^c = \frac{\sigma_C}{E_T} + \beta_T\Delta m + \varepsilon_C^c, \tag{28}$$

where E_L and E_T are the moduli of elasticity along and transverse to the fibre, β_L and β_T are the hygroexpansion coefficients along and transverse to the fibre and Δm is the moisture content change relative a reference level. The strain in section A is given by the fibre model in Section 2.1, Eqs. (2)–(5) and (7),

$$\varepsilon_A = \frac{\sigma_A}{E_L} + \beta_L\Delta m + \varepsilon_A^c + \frac{1}{8}\left(\theta_0^2 - \theta^2\right). \tag{29}$$

The creep strains in the sections A, B and C, $\varepsilon_A^c, \varepsilon_B^c$ and ε_C^c, are given by the creep laws corresponding to Eq. (6)

$$\dot{\varepsilon}_A^c = a_L \sinh\left(b_L\left(\sigma_A - E_L^c\varepsilon_A^c\right)\right), \tag{30}$$

$$\dot{\varepsilon}_B^c = a_L \sinh\left(b_L\left(\sigma_B - E_L^c\varepsilon_B^c\right)\right), \tag{31}$$

$$\dot{\varepsilon}_C^c = a_T \sinh\left(b_T\left(\sigma_C - E_T^c\varepsilon_C^c\right)\right), \tag{32}$$

where a_L, b_L and E_L^c are material parameters in the longitudinal direction of the fibre and a_T, b_T and E_T^c are material parameters transverse to the fibre. The creep strains are assumed to depend only on the stress in the same direction as the creep. This is an approximation, since the strain rate actually depend on the three-dimensional stress state, if that was used some effective stress had to be introduced. The kink angle θ is given by Eqs. (8), (10)–(13),

$$\theta = \theta_0 + \theta_c - \frac{Al^2}{2q_kE_LI}\sigma_A\theta - (\beta_T - \beta_L)(\theta_0 + \theta_c)\Delta m, \tag{33}$$

where the kink angle change caused by creep in the spring, θ_c, is given by the creep law corresponding to Eq. (15),

$$\dot{\theta}_c = -K_1 \sinh\left(K_2\left(\frac{Al}{2}\sigma_A\theta + K_3\theta_c\right)\right). \tag{34}$$

The material parameters K_1, K_2, K_3 are defined in Eqs. (16)–(18), but the constants a, b and E_c are replaced by a_L, b_L and E_L^c, the material parameters along the fibre.

2.3. Numerical solution

The developed fibre network model implicitly defines a constitutive relation between specific stresses $\bar{\sigma}_{ij}^w$ and strains $\bar{\varepsilon}_{ij}$ on the paper (network) level, where i and j takes the values 1 and 2 denoting coordinate directions in the plane of the paper. When the moisture is changed, the hygroexpansive strains at the bonds of the two crossing fibres will be different, i.e. in sections B and C, see Fig. 4, as the hygroexpansion coefficients along and transverse fibres are different. However, since a perfect bonding is assumed, the strains are constrained according to Eq. (21), and the mismatch in hygroexpansive strains must therefore be compensated by elastic

strains and creep strains, according to Eqs. (27) and (28). Elastic strains are generated immediately, producing large stresses. These stresses are added to stresses produced by the external loads on the paper. This gives a stress state where the absolute value of the stresses are higher than before in some parts of the fibres, section B if the moisture is increased and the fibre is loaded in tension, and section C if the moisture is decreased or the fibre is loaded in compression. In the other section of the bonds the absolute value of the stresses are lower than before, i.e. section C if the moisture is increased and the fibre is loaded in tension and section B if the moisture is decreased or the fibre is loaded in compression. However, the mean stress in the fibre segment is practically unchanged, i.e. the stress in the free fibre segment, section A, is rather constant. As the creep laws, Eqs. (30)–(32), are non-linear in stress, i.e. an increase in stress leads to an increase in creep strain rate that is higher than proportional to the stress increase, the increase in creep rate in the bonded parts with high stresses is larger than the decrease in the bonded parts with low stresses. This will lead to an increased mean strain rate, i.e. an acceleration of creep. The stresses relax, even out, as creep takes place and gradually the creep decreases by the stress relaxation as a consequence of the non-linear creep law, thus cyclic moisture content is needed to maintain the accelerated creep over a long time. In order to evaluate the relation between specific stresses $\bar{\sigma}_{ij}^{\mathrm{w}}$ and strains $\bar{\varepsilon}_{ij}$ on the network (paper) level, all internal stress and strain variables must be eliminated. There is however not room here for a detailed explanation of the numerical process. Only the principal steps will be explained. Further details are found in Appendix A4.

It is not possible to solve the non-linear (differential) equations analytically, it is therefore necessary to discretise the problem and solve for a finite number of fibre angles. The fibre angle α is discretised according to

$$\alpha_n = \frac{(n-1)}{N}\pi, \quad n = 1, 2, \ldots, N, \tag{35}$$

where N is a sufficiently large number. The paper is assumed to be isotropic, i.e. the fibre angle is uniformly distributed and all fibres are assumed to have the same properties, dimensions and initial kink angle θ_0. The variables that depend on the fibre angle α are discretised in the same way, i.e. $\varepsilon_n, \varepsilon_{\mathrm{A}n}, \varepsilon_{\mathrm{B}n}, \varepsilon_{\mathrm{C}n}, \varepsilon_{\mathrm{A}n}^{\mathrm{c}}, \varepsilon_{\mathrm{B}n}^{\mathrm{c}}, \varepsilon_{\mathrm{C}n}^{\mathrm{c}}, \sigma_{\mathrm{A}n}, \sigma_{\mathrm{B}n}, \sigma_{\mathrm{C}n}, \theta_n, \theta_n^{\mathrm{c}}$. Furthermore, the macroscopic strains and stresses, $\bar{\varepsilon}_{ij}$ and $\bar{\sigma}_{ij}^{\mathrm{w}}$, constitute six additional variables. The network is thereby described by $12N+6$ variables.

The previously derived equations define, for each angle α, algebraic and differential equations for the different variables. Integrals that appear in the model may be estimated from the corresponding discretised variables. A careful evaluation reveals that there are as many equations as unknowns if for example the stresses $\bar{\sigma}_{ij}^{\mathrm{w}}$ on the macroscopic level are prescribed. Since many of the equations are linear, this feature can be utilized in order to eliminate certain variables. Even though many equations are linear, not all are, for example the differential equations (30)–(32). The equations were therefore solved with iterative methods in MATLAB (2006) using standard routines for solving differential equations and non-linear equations. This is however a more technical question and it does not influence the results. Different combinations of loading, in terms of applied macroscopic stresses $\bar{\sigma}_{ij}^{\mathrm{w}}$ and changes in moisture content Δm as functions of time, can hence be evaluated. Of primary interest is usually the network strains $\bar{\varepsilon}_{ij}(t)$, but other internal variables like the kink angle $\theta(t)$ follow from the analysis.

3. Experimental procedures

All experimental data used in this study were provided by STFI-Packforsk and all tests were performed on the same type of kraft paper produced at STFI-Packforsk, see description about the material and experiments below.

3.1. Material

The raw material for producing the paper material that was studied in this work was a flash-dried unbleached kraft pulp with a Kappa number of 35. The slushed pulp was refined to 21.1° SR (WRV 1.55). The paper was produced in the EuroFEX pilot paper machine at STFI-Packforsk, using a roll former headbox, a lip opening of 13 mm, a forming concentration of 8.2 g/l, a machine speed of 400 m/min, and a jet-wire speed difference of 20 m/min. Standard fabrics and felts were used. The wet pressing was performed in three

nips; a first double-felted roll press nip with a line load of 60 kN/m followed by two single-felted shoe presses with line loads 900 kN/m and 1000 kN/m, respectively. A dryness of 44.6% was reached after the last press. The paper web was wound up after wet pressing and was dried off-line under in-plane biaxial constraint in STFI-Packforsk's one-cylinder dryer. The dried paper samples were relaxed by exposing them to a climate of 23 °C and a cyclic relative humidity (RH) ranging between 50% and 90% before material testing was performed. Three cycles in relative humidity, each with a duration of seven hours, were used. The produced paper had a grammage of 100 g/m^2 and a structural thickness of 0.121 mm.

3.2. Hygroexpansivity testing

The hygroexpansivity tests were performed at STFI-Packforsk using a recently developed custom made apparatus that allows for measurement of the in-plane dimensions of paper tests specimens in a controlled climate environment. The apparatus is equipped with an anti-buckling device, which makes it possible to measure hygroexpansivity without applying in-plane loading. The test specimens were 15 mm wide and a clamping length of 100 mm was used. A test piece was placed on a horizontal test table with hydrophobic surface and was clamped between two grips. One of the grips was rigidly mounted on the test table, while the other grip was mounted on a smooth-running sled. The moisture-induced changes in length of the test piece were measured by recording the movement of the sled. Measurements for up to 30 specimens may be performed simultaneously. The in-plane dimensions of the test specimens were measured at 23 °C and at four different ambient relative humidities in the range from 50% RH to 90% RH. The measurements were performed in both the MD and CD after that the tests specimens had reached moisture equilibrium, although in this study only the results in MD are used.

3.3. Tensile testing

The tensile testing of the studied paper material was performed at STFI-Packforsk in a climate room using a L&W Tensile Tester. The tensile testing was performed in both the machine direction (MD) and cross-machine direction (CD) following ISO 1924-3, although in this study only the results in MD are used. Furthermore, the testing was performed for conditioned paper specimens in 23 °C and 50% RH as well as in 23 °C and 90% RH. The test pieces used were 15 mm wide and the clamping length was 100 mm. A constant strain rate of 1.67%/s was used.

3.4. Compressive testing

The compressive testing was performed at STFI-Packforsk in a climate room using a custom made material testing equipment that is designed to prohibit out-of-plane buckling of thin sheet structures during in-plane loading in compression. The equipment utilises a series of opposing columns that provide lateral support of the test specimen without introducing in-plane loading. This equipment is further described by Panek et al. (2004). The width of the test pieces was 25 mm and the clamping length was 55 mm. The applied load was recorded by a load cell and the deformation of the test piece was measured using two LVDT's, each one connected to a surface-contacting needle that monitored displacement of the test specimen. A target strain rate of 0.2%/s was applied manually using a lever and a soft spring until ultimate failure was detected. The compressive testing was performed for conditioned paper specimens in 23 °C and 50% RH as well as in 23 °C and 90% RH and in both the MD and CD, although in this study only the results in MD are used.

3.5. Creep testing

The creep tests were performed in both the MD and CD under tension as well as under compression using the same equipment and test geometry as in the compressive testing. However, in this study only the results in MD are used. The tests were further performed for conditioned paper specimens in 23 °C and 50% RH as well as in 23 °C and 90% RH. The loading was applied by the use of a lever and a dead-weight. Creep testing under various different constant load levels was performed.

3.6. Mechano-sorptive creep testing

The mechano-sorptive creep tests were performed in the MD under tension as well as under compression using the same equipment, test geometry, and method for load application as in the creep testing. The loading was applied to the test piece at 50% RH. The test piece was then subjected to three 7 hour cycles between 50% RH and 90% RH. The RH-cycle was designed so that the climate was kept constant for approximately three hours at each of the limiting relative humidities (50% and 90% RH), while the climate was ramped as rapid as possible in between these limiting relative humidities. Mechano-sorptive creep testing under various different constant load levels was performed.

4. Material parameters

The number of parameters that have been introduced is quite large. They were estimated from experiments, literature or they were calculated, and are listed in Table 1. The parameters generally depend on the moisture content, but in order to illustrate the main features of the model some simplifying assumptions have been made, among other things, the parameters are assumed to be moisture independent. It is also assumed that the anisotropy, i.e. the difference in material parameters along and transverse to the fibre, can be described by a single constant $\eta > 0$, such that

$$\frac{E_{\mathrm{L}}}{E_{\mathrm{T}}} = \frac{E_{\mathrm{L}}^{\mathrm{c}}}{E_{\mathrm{T}}^{\mathrm{c}}} = \left(\frac{a_{\mathrm{L}}}{a_{\mathrm{T}}}\right)^{-1} = \eta. \tag{36}$$

This constant is assumed to be the same for creep parameters as it is for elastic parameters, as can be found in the literature (Schulgasser and Page, 1988; Bergander and Salmén, 2002; Salmén, 2004; Neagu, 2006).

It is assumed that the fibres in the paper are made of softwood, the length, L_{tot}, and width, B, of the fibres are chosen according to that (Niskanen, 1998). The number of fibre bonds can be approximated as (Komori and Makishima, 1977)

$$n(\phi, \xi) = \frac{2V_{\mathrm{f}}L_{\mathrm{tot}}}{B} J(\phi, \xi), \tag{37}$$

where

$$J(\phi, \xi) = \int_0^{\pi} \int_0^{\pi} \Omega(\phi', \xi') \sin\chi(\phi, \xi, \phi', \xi') \sin\phi' \mathrm{d}\xi' \mathrm{d}\phi' \tag{38}$$

for a general three-dimensional problem. Here a rectangular cross section has been assumed instead of the circular cross section that was used in the reference article. It is assumed that the fibre of interest has orientation (ϕ, ξ), where ϕ is the angle between the z-axis and the axis of a fibre and ξ is the angle between the x-axis and the normal projection of the fibre axis onto the xy-plane. The function $\Omega(\phi', \xi')$ is a frequency function for the fibre angle distribution that shall satisfy

$$\int_0^{\pi} \int_0^{\pi} \Omega(\phi, \xi) \sin\phi \mathrm{d}\xi \mathrm{d}\phi = 1, \tag{39}$$

and χ is the angle between the fibre given by the direction (ϕ, ξ) and a fibre given by the direction (ϕ', ξ'). When all fibres are uniformly distributed in the xy-plane, $\phi = \pi/2$, $\xi = \alpha$, $\Omega(\phi', \xi') = f(\alpha)/2$, $f(\alpha) = 1/\pi$ and $\sin\chi = |\sin(\alpha - \alpha')|$. This inserted into Eq. (38) gives

$$J(\alpha) = \frac{1}{\pi} \int_0^{\pi} |\sin(\alpha - \alpha')| \mathrm{d}\alpha' = \frac{2}{\pi}. \tag{40}$$

If this value of J is inserted in Eq. (37), the number of fibre bonds can be approximated as,

$$n(\phi, \xi) = \frac{4V_{\mathrm{f}}L_{\mathrm{tot}}}{\pi B}, \tag{41}$$

Table 1
Parameters used in the network model

Parameter	Value	Comment
L_{tot}	3.5 mm	Length of fibres (Niskanen, 1998)
B	35 μm	Width of the bars/fibres (Niskanen, 1998)
H	5 μm	Height of the bars/fibres (Niskanen, 1998)
ρ_f	1500 kg/m^3	Fibre density (Niskanen, 1998)
ρ_p	826 kg/m^3	Paper density, from experiments
V_f	$\rho_p/\rho_f \approx 0.55$	Volume fraction of fibres
n	$\frac{4V_f L_{tot}}{\pi B}$	Number of fibre bonds. The number of fibre segments used here is $n-1$
L	50 μm	Total length of fibre segment, calculated from L_{tot}
λ	$\frac{L_f}{L} = \frac{L-B}{L} = 0.30$	Length of free fibre segment divided by total length of fibre segment
L_f	$\lambda L = 15$ μm	Length of free fibre segment
l	$L_f/2 = 7.5$ μm	Length of one bar
A	$BH \approx 1.75 \times 10^{-10}$ m^2	Fibre cross section area, here a rectangular cross section has been assumed
I	$\frac{BH^3}{12} \approx 3.65 \times 10^{-22}$ m^4	Moment of inertia, here a rectangular cross section has been assumed
η	6	Anisotropy constant (Schulgasser and Page, 1988; Bergander and Salmén, 2002; Salmén, 2004; Neagu, 2006)
E_L	44 GPa	Modulus of elasticity along the fibre, estimated from experimental stress–strain curves in tension and creep curves at $t = 0$
E_T	$E_L/\eta \approx 7.3$ GPa	Modulus of elasticity transverse to the fibre, calculated from Eq. (36)
β_L	0.013	Hygroexpansion coefficient along the fibre, estimated from experimental hygroexpansion data
β_T	$20\beta_L = 0.26$	Hygroexpansion coefficient transverse to the fibre (Niskanen, 1998)
θ_0	6.6°	Initial kink angle, estimated from the method described in Section 4
a_L	3×10^{-8} s^{-1}	Constant in the creep law along the fibre, see Eqs. (30), (31), estimated from regular creep curves in tension
b_L	9×10^{-8} Pa^{-1}	Constant in the creep law along the fibre, see Eqs. (30), (31), estimated from regular creep curves in tension
E_L^c	4 GPa	Constant in the creep law along the fibre, see Eqs. (30), (31), estimated from regular creep curves in tension
a_T	$\eta a_L = 1.8 \times 10^{-7}$s^{-1}	Constant in the creep law transverse to the fibre, see Eq. (32), calculated from Eq. (36)
b_T	$b_L = 9 \times 10^{-8}$ Pa^{-1}	Constant in the creep law transverse to the fibre, see Eq. (32)
E_T^c	$E_L^c/\eta \approx 0.67$ GPa	Constant in the creep law transverse to the fibre, see Eq. (32), calculated from Eq. (36)
q_k	0.044	Constant in the equation for the torsional spring constant, Eq. (11), estimated from experimental stress–strain curve in compression and creep curves at $t = 0$
k_1	100	Constant in the creep law for the spring, see Eqs. (16), (14), estimated from regular creep curves in compression
k_2	100	Constant in the creep law for the spring, see Eqs. (17), (14), estimated from regular creep curves in compression
k_3	0.01	Constant in the creep law for the spring, see Eqs. (18), (14), estimated from regular creep curves in compression
N	18	Number of fibres in the model. One fibre for every 10°, approximated the uniform distribution well
$\bar{\sigma}$	$[\sigma^w \quad 0 \quad 0]^T$ kNm/kg	Macroscopic specific stresses in the paper, for stress levels see the individual plots
m_{ref}	0.07	Starting moisture content. Estimated from the experimental value 50% RH (Byrd, 1972a; Gellerstedt, 2004)
m_{max}	0.15	Maximum moisture content. Estimated from the experimental value 92% RH (Byrd, 1972a; Gellerstedt, 2004)
m_{min}	0.07	Minimum moisture content. Estimated from the experimental value 50% RH (Byrd, 1972a; Gellerstedt, 2004)

and the number of fibre segments can be approximated as $n-1$. The fibre segment length L can then be estimated from the total fibre length L_{tot}.

Experimental experience from an automatic measuring method based on image analysis called STFI Fiber-Master (Karlsson and Fransson, 1994) at STFI-Packforsk shows that there is in average one kink (or angular fold) per fibre in a paper. The observed average kink angle is about 50°. The average kink angle has also been approximated from an article by Mohlin et al. (1996) where, if the number of kinks and/or angular folds is known the number of twists (torsional deformation) can be approximated. If the sum of all three fibre deformations is known the shape factor can be approximated from the article. The shape factor is the ratio between

the length of the diagonal in the circumscribed rectangle and the length of the fibre. The shape factor is sensitive to the number of deformations that change the direction of the fibre axis, and the dependence has been experimentally determined in the article. If the sum of kinks and angular folds is in average one, the sum of deformations is approximately 1.5, which gives a shape factor that is approximately 89%. From the shape factor the kink angle can be approximated to be about 60°.

In the network model it is assumed that all free fibre segments have a kink, not only one kink per fibre. A suitable kink angle per free fibre segment θ_0 has to be found that gives a similar response as a fibre with only one large kink. The fibre model described in Section 2.1 was applied. Only elastic deformation was considered. The number of fibre segments is estimated by use of Eq. (41). The stress–strain curve for a fibre with one fibre segment with a large kink, here 55° was used, and the other fibre segments were straight, was compared to the stress–strain curve for a fibre where all free fibre segments had the same small kink angle θ_0. The kink angle in the last model, θ_0, was changed until a good agreement between the two curves was found, special consideration to the agreement for small loads was taken. The kink angle found in this way was then used in the network model as θ_0.

The fibre network model that was derived in the paragraphs above implicitly defines a constitutive relation between specific stresses $\bar{\sigma}^{\mathrm{w}}_{ij}$ and strains $\bar{\varepsilon}_{ij}$ on the paper level. These equations were solved in MATLAB (2006) using standard routines for solving differential equations and non-linear equations. The values of the parameters in the model were estimated from experiments, literature or they were calculated, see Table 1. A few parameters, $E_{\mathrm{L}}, q_{\mathrm{k}}, \beta_{\mathrm{L}}, a_{\mathrm{L}}, b_{\mathrm{L}}, E^{\mathrm{c}}_{\mathrm{L}}, k_1, k_2, k_3$, were fitted to experimental data. All experimental data used were provided by STFI-Packforsk and all tests were performed on the same type of kraft paper produced at STFI-Packforsk, see Section 3. Although the model is isotropic on paper level while the real paper is anisotropic, it can still be used for qualitative comparisons. In the mechano-sorptive creep experiments the relative humidity was varied between 50% and 92%. This corresponds approximately to moisture contents of 7% at 50% RH and 15% at 92% RH, respectively (Byrd, 1972; Gellerstedt, 2004). The macroscopic specific stress prescribed along the 1-axis is set to $\bar{\sigma}^{\mathrm{w}}_{11} = \sigma^{\mathrm{w}}$, where σ^{w} is the value used in the experiment of current interest. When the stress and the moisture history are set the strains are calculated. A principal sketch of mechano-sorptive creep in both tension and compression is shown in Fig. 7.

The modulus of elasticity along the fibre, E_{L}, affects the elastic behaviour of the paper, and it controls the strain at point a in Fig. 7. Because the moisture dependence of E_{L} is ignored, the value of E_{L} used in the model is the mean value between the value at 50% RH and 90% RH. To find a suitable value of E_{L}, the model, but only with elastic terms, i.e. no moisture variations or creep, was fitted to data in the region of 0–15 kNm/kg from the stress–strain curves, see Fig. 8.

The constant q_{k} in the equation for the elastic torsional spring constant affects the elastic response of the kink angle, i.e. it influences mostly the elastic behaviour of the paper under compression, and can approximately be seen as the difference between the strain at point b and point a in Fig. 7. To estimate q_{k}, data in

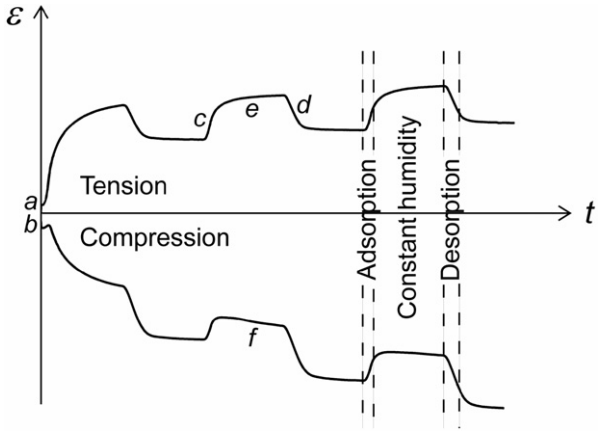

Fig. 7. A principal sketch of mechano-sorptive creep in both tension and compression.

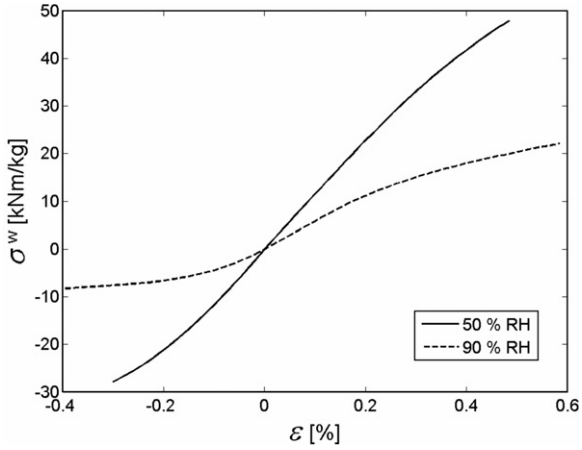

Fig. 8. Stress–strain curve composed of data from fast tension and compression tests at 50 and 90% RH, i.e. the paper should behave elastically. The curves are a mean value from approximately ten tests in tension and ten tests in compression for each relative humidity.

the region of negative stress level down to −15 kNm/kg from the stress–strain curves was used, see Fig. 8. Only elastic terms in the model were used, i.e. no moisture variations or creep. After a suitable value of q_k was found, the fit was inspected for positive stress values in the stress–strain curve, see Fig. 8, so that no large changes had appeared in elastic tensile behaviour.

The hygroexpansion coefficient along the fibre, β_L, affects the response of the paper when the moisture content is changed, and can be seen as the strain change in area c and d in Fig. 7. To find a suitable value of β_L, the model, but only with hygroexpansive strains, i.e. no applied load, was fitted to the hygroexpansion data, shown in Fig. 9. The moisture content was estimated from the relative humidity using the relationship given above.

After the constants that affect the elastic and hygroexpansive behaviour of the creep curve have been estimated, the constants in the creep law along the fibre, a_L, b_L, E_L^c, can be approximated. These constants affect the creep properties of the paper and can be viewed as the change in strain in area e in Fig. 7, i.e. when the moisture content is constant. The model, with constant moisture content, was fitted to the creep curves at different tensile loads and relative humidities of 50% RH and 90% RH, see Fig. 10. The experimental curves used were those with approximately the same load at both relative humidity levels, i.e. the curves with stresses 3.6, 5.5/5.3 kNm/kg, which also are stress levels used in the mechano-sorptive creep tests. The parameter E_L^c affects the creep curve from the beginning of the curve, i.e. the elastic response, but a change can be noted throughout the entire curve. If E_L^c is increased the creep decreases. The parameters a_L and b_L on the other hand do not affect the elastic behaviour noticeably, but the following creep behaviour. If these parameters are increased the creep is increased. A small change in b_L affects the curve more than a change in a_L and b_L affects the curve mostly at small times, while a_L affects the creep curve for mostly for larger times. It should be noted that the time scale used in the regular creep tests (∼0–300 s) are unfortunately not the same as the one used for mechano-sorptive creep tests (∼0–70 000 s), which makes the fitting much more difficult.

The constants k_1, k_2, k_3, that appear in the creep law for the spring, affect the creep response of the kink angle, i.e. they influence mostly the creep behaviour of the paper under compression, and can approximately be seen as the difference between the changes in strain in areas e and f, as shown in Fig. 7. The model was fitted to the creep curves at different compressive loads and relative humidities of 50% RH and 90% RH, see Fig. 11. More specifically, the experimental curves used were those with approximately the same load at both relative humidity levels, i.e. the curves with the specific stresses −2.6, −4.7 kNm/kg at 50% RH and the specific stresses −2.4, −4.4 kNm/kg at 90% RH were considered. These stress levels are at the same order as those that were applied in the mechano-sorptive creep tests. Again it should be noted that the time scale used in the regular creep tests are not the same as the one used for mechano-sorptive creep tests. After suitable values of k_1, k_2, k_3 were found, the model was inspected against the creep curves at different tensile loads, shown in Fig. 10, so that no large changes have appeared in tensile creep behaviour.

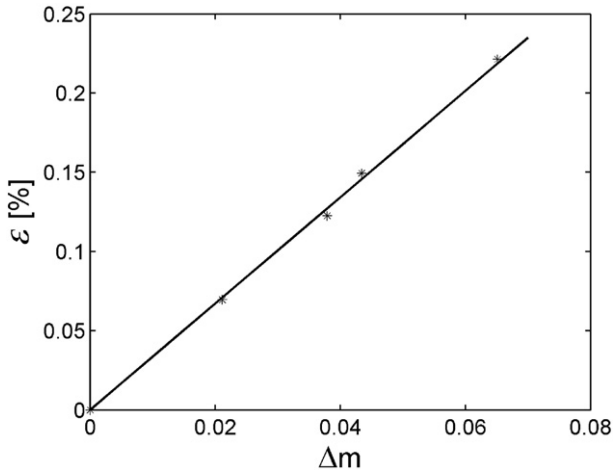

Fig. 9. Hygroexpansive strains vs. relative moisture content changes. The stars represent experimentally determined strains, were each star is a mean value from around ten test specimens. The relative humidity was varied between 50% and 84%. The line is the fit with the model.

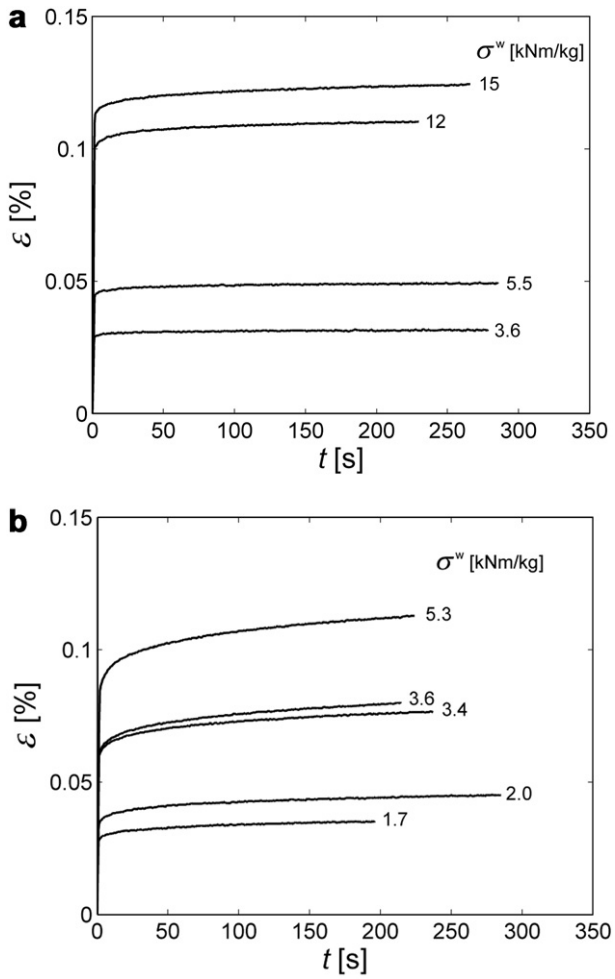

Fig. 10. Experimental creep curves with different tensile specific stresses at 50% RH (a) and 90% RH (b).

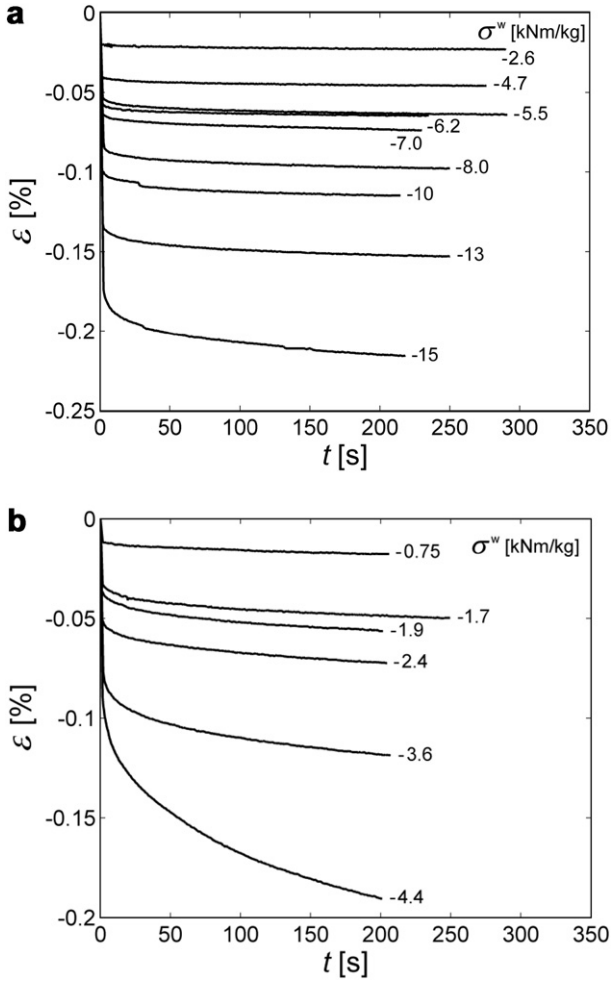

Fig. 11. Experimental creep curves with different compressive specific stresses at 50% RH (a) and 90% RH (b).

5. Results and discussion

In Fig. 12, experimental mechano-sorptive creep curves under both tensile and compressive loading are presented. It can be observed that the paper creeps much faster in compression, which leads to more deformation at a given time and stress level. Mechano-sorptive creep curves determined from the present model are shown in Fig. 13. It can be seen that the model can capture mechano-sorptive creep both under tension and compression, as well as the differences between these two load cases, but the difference is not as pronounced as the experimental curves show. In Fig. 12(a) it is shown how the relative humidity was varied during the experiments, and in Fig. 13(a) it can be seen how the moisture content was varied in the model. If the moisture curve is changed, for example if the ramp time is increased or if the moisture is varied sinusoidally it does not affect the results from the model. The shape of the mechano-sorptive curve follows the shape of the moisture curve, but the strain after each cycle is the same. Gunderson and Tobey (1990) carried out creep tests in cyclic relative humidity on paperboard in tension and compared different cyclic humidity conditions, the ramp time and hold time was varied so that the moisture curve was changed between sine shaped to steep step shaped. They presented similar experimental results where the deformation after a given number of cycles was almost the same, independent of the ramp time and hold time. However, in their creep tests moisture equilibrium cannot be assured for all moisture curves.

In Fig. 14, the mechano-sorptive creep curves from experiments (a) and the model (b) are compared for a specific stress level, both under tensile loading and compressive loading. Because the experiments under

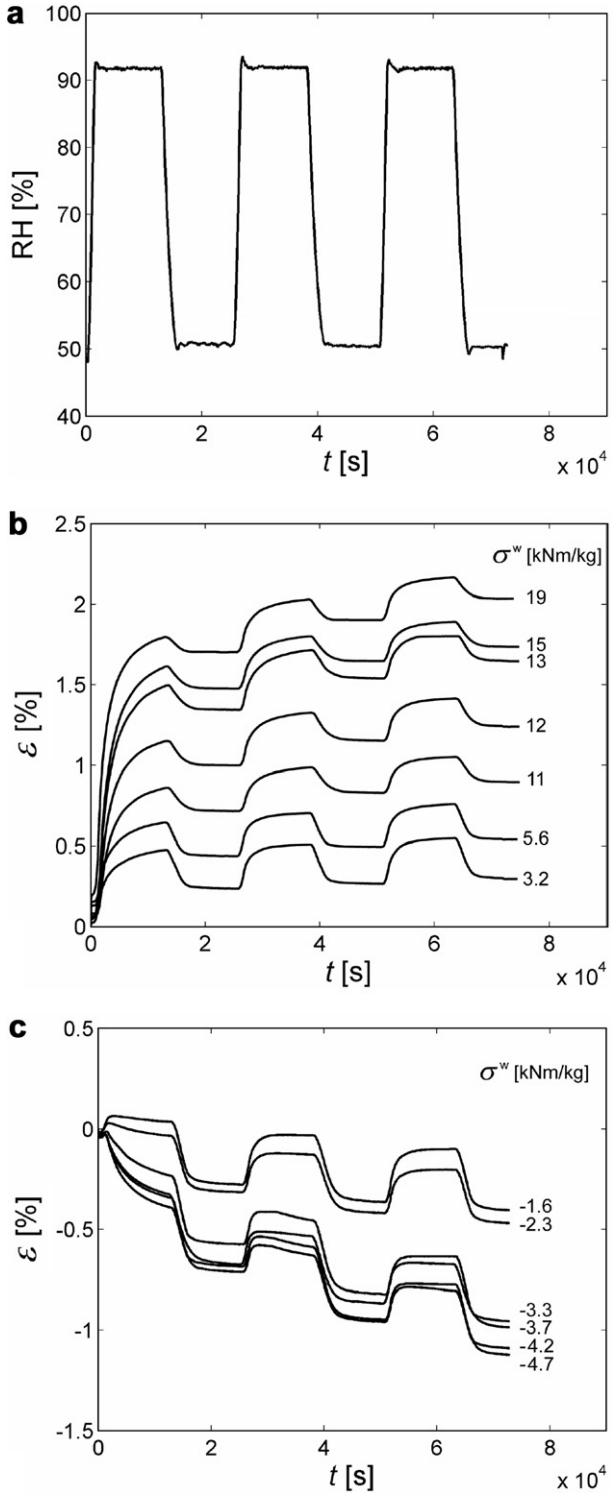

Fig. 12. Experimental mechano-sorptive creep curves where the relative humidity was varied as shown in (a). Tests were performed both with tensile (b) and compressive specific stresses applied (c).

tension were not performed at the same stress levels as under compression, interpolation has been used between two curves (3.2 kNm/kg and 5.6 kNm/kg) to receive the curve in tension. This gives an approx-

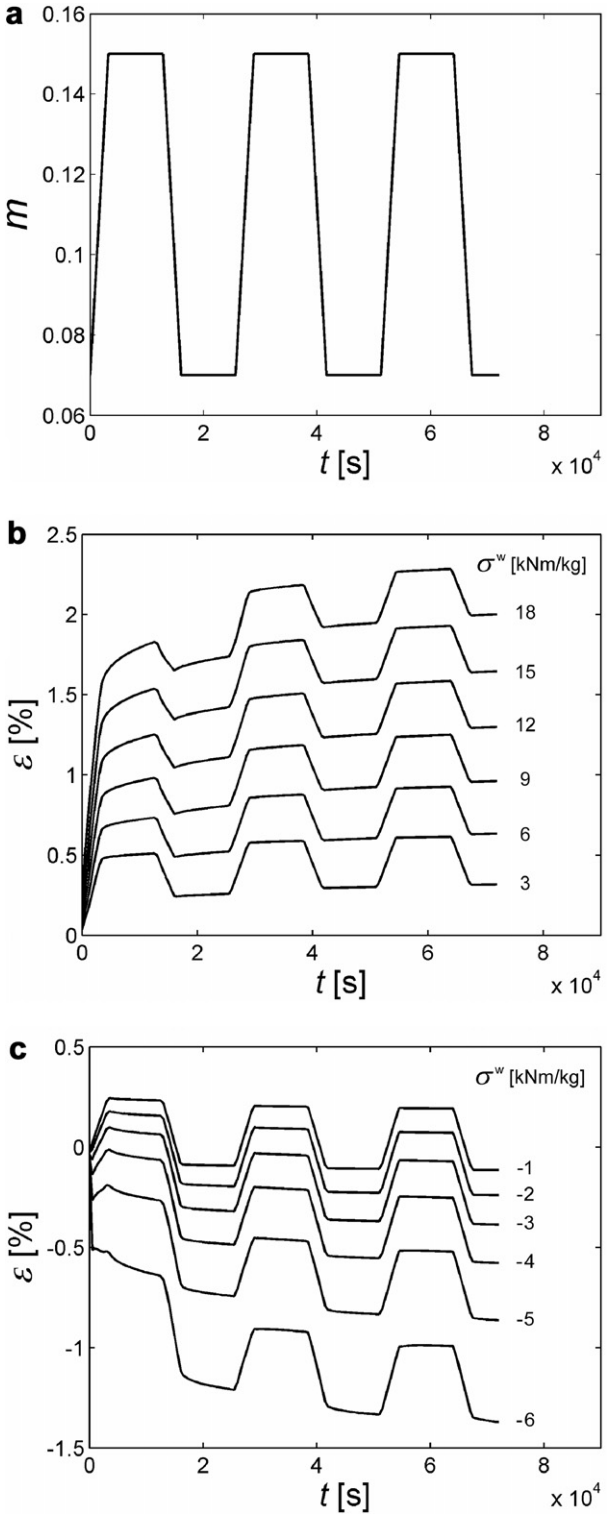

Fig. 13. Mechano-sorptive creep curves from the model where the moisture content was varied as shown in (a). Results from simulations with both tensile (b) and compressive specific stresses applied (c).

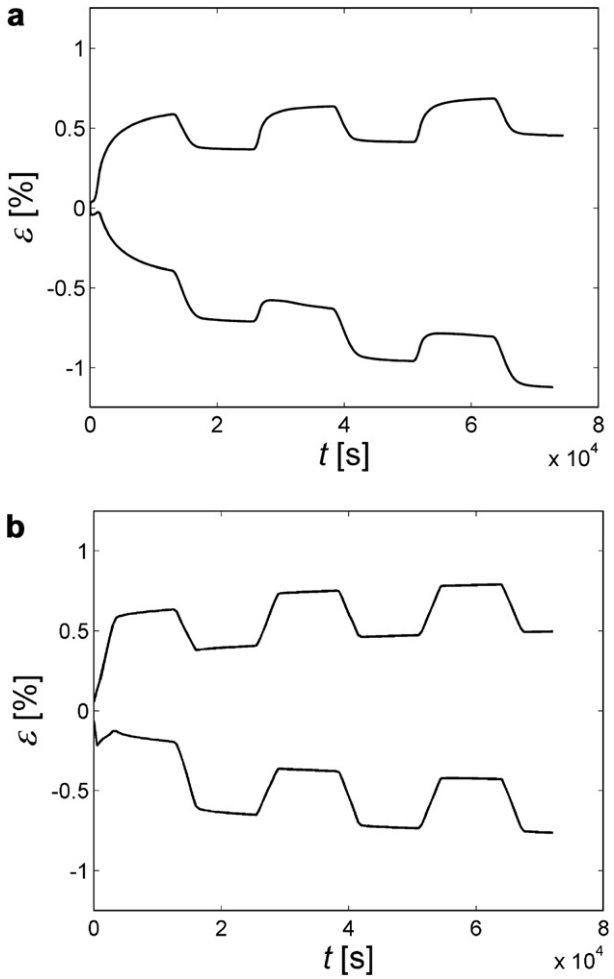

Fig. 14. Mechano-sorptive creep curves from experiments (a) and the model (b), where the same stress has been used in tension and compression, 4.7 kNm/kg.

imate curve that is useful for comparison, although the strain is not linearly dependent on the stress. The predicted hygroexpansion is larger than the experimental one, both in tension and in compression. The predicted creep in compression is however smaller, which explains the smaller difference between tension and compression resulting from the model. It should be noted that the moisture change used here is positive, which makes it harder to see that the mechano-sorptive effect is larger in compression. The experimental creep curves show smoother transitions between small and large moisture contents compared to the predicted creep curves. This can be explained by the applied moisture content profile in Fig. 13(a). In the experiments it can be assumed that the moisture content slowly changes until it reaches the equilibrium level.

By the shape of the curves it can also be seen that the applied creep law is not perfect. The creep rate defined by the creep law has a tendency to decrease too fast. Another creep law, especially for the torsional spring, could also affect the difference in mechano-sorptive creep with tensile and compressive loading. Unfortunately the relative humidity was only cycled three times during the mechano-sorptive creep experiments, with more cycles the long time creep behaviour would be more prominent and it would be easier to compare the results from the model to the experimental results. It should be kept in mind that the material parameters used in the model were assumed to be constant, while they actually should be moisture dependent. In the plots from the experiments differences can be seen for low and high mois-

ture content, for example that the creep rate is higher for the high moisture level, which is not captured by the model.

In Fig. 15, predicted mechano-sorptive creep curves are compared to curves where simply the contribution from a pure hygroexpansion test and a regular creep test has been added. Curve a is a hygroexpansion curve, curves b and c are creep curves in tension and compression, curves d and e are these contributions added, i.e. $a+b$ and $a+c$, which should be compared to the mechano-sorptive creep curves f and g. It can be concluded that the strain caused by mechano-sorptive creep is larger than the strain from the contributing parts, i.e. the strain from a test with only moisture expansion is added to the strain from a test with only load applied. Hence, it is evident that accelerated creep is obtained by the model. This can also be seen if the regular creep curves (b and c) are compared to the mechano-sorptive creep curves (f and g) at the reference moisture content level. Only a very small divergence can be seen if the difference between curves d and f are compared to the difference between curves e and g, which has to do with the difference in hygroexpanision if a tensile or a compressive load is applied, an effect of the moisture dependence in the spring. Hence, the larger mechano-sorptive creep in compression is an effect of the extra hygroexpansion, elastic deformation and creep in compression compared to tension, that depends on the fibre model. The additional elastic deformation and creep deformation can be observed in the regular creep curve.

If the fibres in the model were modelled as straight, the paper properties would be the same in compression and tension. In Fig. 16, mechano-sorptive creep in tension and compression is showed for a specific stress level (5 kNm/kg), both with kinked fibres and with straight fibres. It can be seen that the kinks affect the deformation under tension, but much more under compression, which leads to a more compliant behaviour in compression. If the difference in strain between points A and B is compared to the difference in strain between point D and E it can be seen that the paper creep is larger in compression than in tension. If instead the difference in strain between points B and C is compared to the difference in strain between point E and F it can be seen that the hygroexpanison is larger in compression than in tension. Unfortunately the elastic strain can not be compared since the moisture content is changed directly, but the model produces larger elastic strain in compression compared to tension.

From mechano-sorptive creep curves at different stress levels, isocyclic stress–strain curves can be plotted, see Fig. 17. Hence the strain after a certain number of moisture cycles (here three) is registered as a function of stress. There is a good agreement between experimental data and the isocyclic curve from the model. Both experiments and theory show a more compliant behaviour in compression compared to tension.

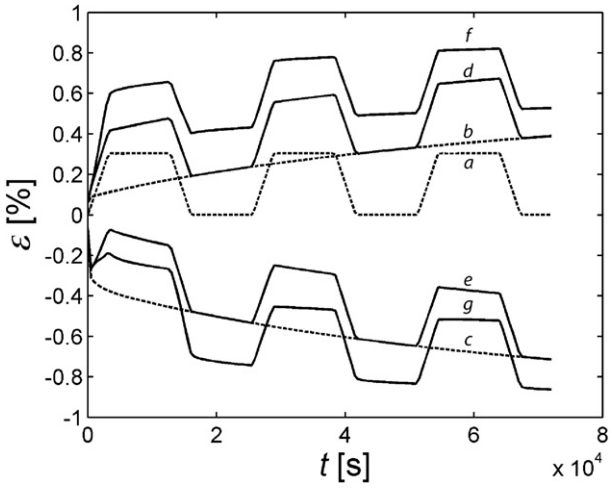

Fig. 15. Comparison between the mechano-sorptive creep curve (curves f and g) and the curve if the contribution from a hygroexpansion test (curve a) and a regular creep test (curves b and c) are added (curves d and e). The specific stress used is 5 kNm/kg.

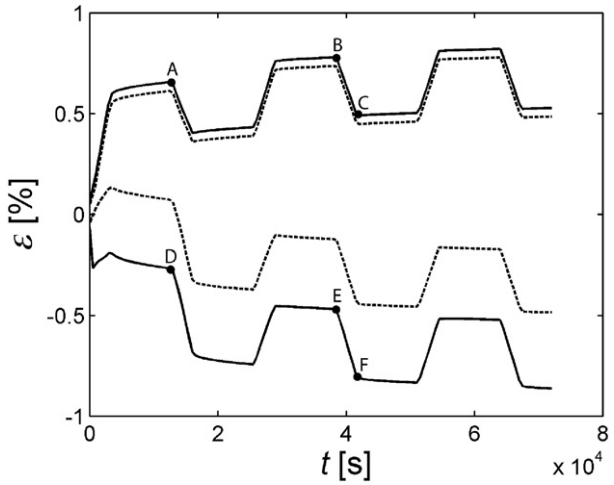

Fig. 16. Comparison between mechano-sorptive creep curves from the model, where kinked (—) and straight (···) fibres have been used. The specific stress used is 5 kNm/kg.

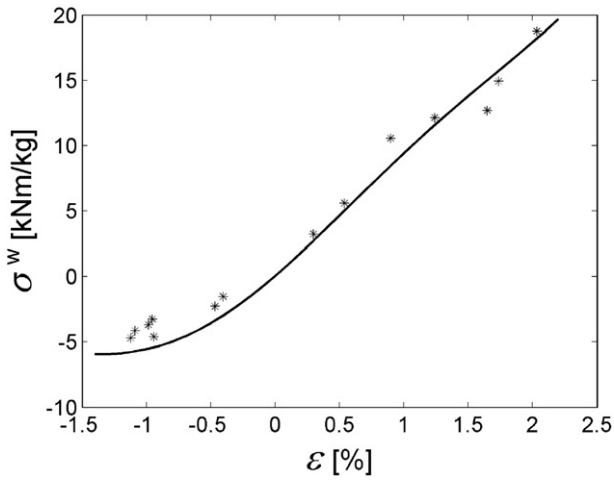

Fig. 17. Isocyclic data from experiments (∗) and from the model (—) after three cycles (7.2×10^4 s).

6. Conclusions

In this paper a simplified network model for mechano-sorptive creep has been developed. It is assumed that the anisotropic hygroexpansion of the fibres produces large stresses at the fibre-fibre bonds when moisture changes. The resulting stress state will accelerate creep if the material obeys laws that are non-linear in stress. During creep the stresses created at the bonds relax, and the moisture content has to change again to maintain the accelerated creep. Geometrical fibre effects, such as kinks, are included in order to capture experimental observations of the differences between paper loaded in tension and compression. Material parameters in the micromechanical model are estimated from experimental results, such as stress–strain curves, hygroexpansion curves and regular creep curves. Theoretical predictions based on the developed model are compared to experimental mechano-sorptive creep curves for paper both under tensile and compressive loading at varying moisture content. There are some differences in the curves from experiments and the model, but the important features are captured. This shows that accelerated creep is obtained by the model without adding extra mechanisms. There could be some differences, in for example the bonds, during accelerated creep compared to con-

stant creep that is not included in this model. Such differences could possibly cause extra acceleration of the creep, but is not necessary to obtain accelerated creep. The model could however be improved by further examination and better modelling of the fibre bonds and also by introducing effects of microcompressions. The creep predicted by the model is accelerated by the moisture cycling and the important difference between mechano-sorptive creep in the two load cases is captured, i.e. the mechano-sorptive effects are larger in compression than in tension. This is a strong indication that fibre kinks and curl are the main reason for the differences in tension and compression. The model could be improved by changing the creep law, but unfortunately no better creep law for fibres are available at the moment. The creep law used may have improved performance and/or physical meaning if the creep constants could be determined using the physical mechanisms behind the model as described by Eyring, instead of curve fitting. The model could also be improved by introducing anisotropy and moisture dependent material parameters.

Acknowledgments

The financial supports from Biofibre Materials Centre (BiMaC) and the Paper Mechanics cluster at STFI-Packforsk are gratefully acknowledged. The authors are also grateful to Dr. Johan Alfthan for valuable discussions and to Tech. Lic. Petri Mäkelä at STFI-Packforsk for providing experimental results.

Appendix A. Estimation of material parameters

A.1. Estimation of the torsional spring constant k

As mentioned earlier, the fibres are modelled as bars connected by torsion springs, as shown in Fig. A1. It is first assumed that the fibres only deform elastically, i.e. the kink angle θ consists partly of the initial angle θ_0, and partly of the elastic angle θ_e,

$$\theta = \theta_0 + \Delta\theta = \theta_0 + \theta_e. \tag{A1}$$

The elastic angle change is linearly dependent on the torsional spring moment, M,

$$\theta_e = \Delta\theta = \frac{M}{k}, \tag{A2}$$

where k is the torsional spring constant. To estimate the elastic torsional spring constant, the fibre model is approximated by beams that bend, see Fig. A2.

The kink angle can then be approximated as

$$\Delta\theta = 2\Delta\varphi \approx 2\frac{\delta}{l} \approx 2\frac{Fl^2}{3EI} \approx \frac{2Ml}{3EI}. \tag{A3}$$

Solving Eqs. (A2) and (A3) for the torsional spring constant k gives

$$k \approx \frac{3}{2}\frac{EI}{l}, \tag{A4}$$

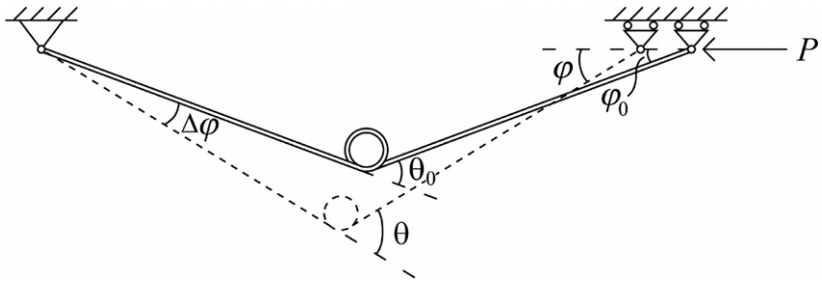

Fig. A1. The fibre model in an initial state and a deformed state.

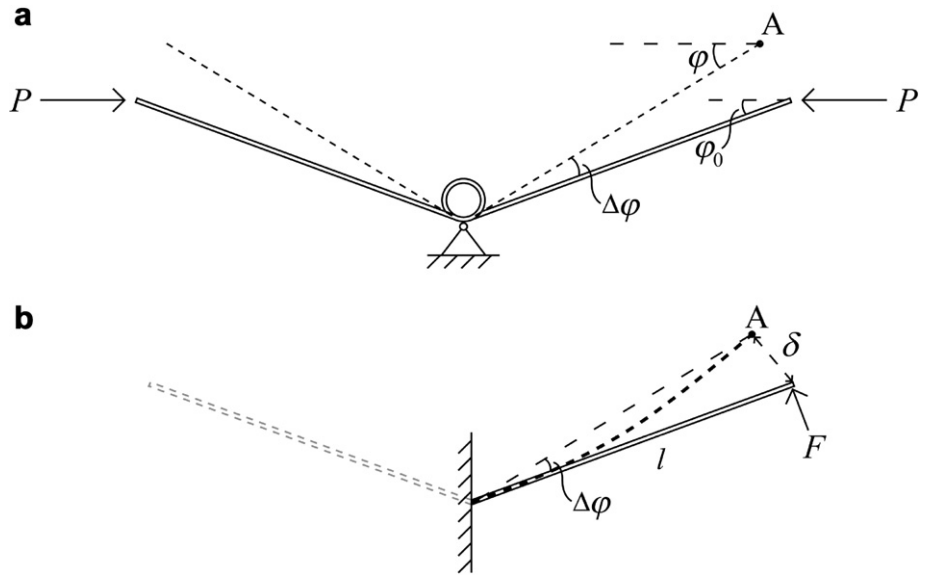

Fig. A2. The torsional spring in the fibre model (a) is defined so that the change in angle $\Delta\varphi$ is the same as that for bending of corresponding kinked beams (b).

i.e. a reasonable estimation of the torsional spring constant is

$$k = q_{\mathrm{k}} \frac{EI}{l}, \tag{A5}$$

where q_{k} is a non-dimensional constant.

A.2. Estimation of hygroexpansion coefficient for the kink angle β_m

The hygroexpansion coefficient for the kink angle can be estimated from the hygroexpansion coefficients for the fibre, along and transverse to the fibre axis. When the moisture content in the fibre changes Δm, the fibre strain along and transverse to the fibre axis is given by

$$\Delta\varepsilon_{\mathrm{L}} = \beta_{\mathrm{L}}\Delta m, \tag{A6}$$

$$\Delta\varepsilon_{\mathrm{T}} = \beta_{\mathrm{T}}\Delta m, \tag{A7}$$

where β_{L} and β_{T} are the hygroexpansion coefficients for the fibre, along and transverse to the fibre axis, respectively, and $\beta_{\mathrm{T}} > \beta_{\mathrm{L}}$. To simplify the following analysis, the hygroexpansion can be divided into two steps:

$$\text{Step1} : \Delta\varepsilon_{\mathrm{L}}^{1} = \Delta\varepsilon_{\mathrm{T}}^{1} = \beta_{\mathrm{L}}\Delta m \tag{A8}$$

$$\text{Step2} : \Delta\varepsilon_{\mathrm{L}}^{2} = 0, \quad \Delta\varepsilon_{\mathrm{T}}^{2} = (\beta_{\mathrm{T}} - \beta_{\mathrm{L}})\Delta m \tag{A9}$$

which fulfil the requirement given by Eqs. (A6) and (A7),

$$\Delta\varepsilon_{\mathrm{L}} = \Delta\varepsilon_{\mathrm{L}}^{1} + \Delta\varepsilon_{\mathrm{L}}^{2} = \beta_{\mathrm{L}}\Delta m, \tag{A10}$$

$$\Delta\varepsilon_{\mathrm{T}} = \Delta\varepsilon_{\mathrm{T}}^{1} + \Delta\varepsilon_{\mathrm{T}}^{2} = \beta_{\mathrm{T}}\Delta m. \tag{A11}$$

The first step, where the strain along and transverse to the fibre is equal, defines a pure volume change that does not cause changes in kink angle. In the second step, where the fibre expansion only occurs in the transverse direction, the change in kink angle can be determined from a geometrical consideration. Before the moisture change, the fibre is assumed to have an initial curvature, i.e. a kink angle φ_1 as shown in Fig. A3(b), composed of the initial angle φ_0 and the creep angle φ_{c},

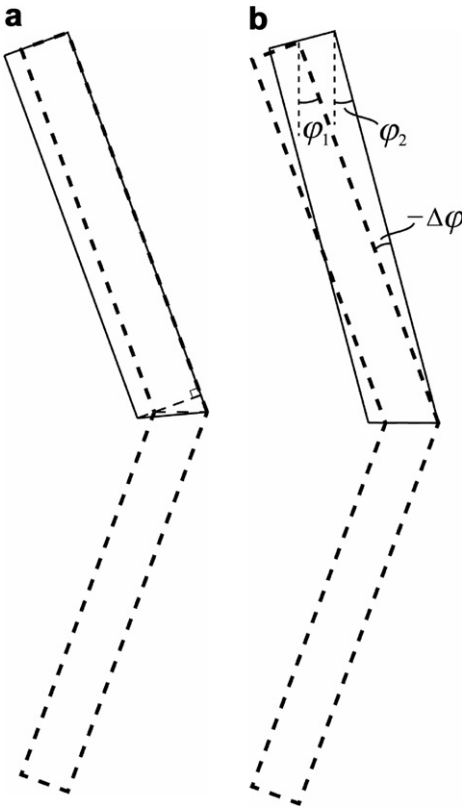

Fig. A3. The fibre expansion if the moisture content is increased. In (a) the expansion of half the fibre is shown if the geometrical effect of the other half is disregarded. In (b) the corrected deformed geometry is considered, when the other half has been taken into consideration. The initial state is drawn with dashed lines and the deformed state with solid lines.

$$\varphi_1 = \varphi_0 + \varphi_c. \tag{A12}$$

The kink angle after moisture change is denoted as φ_2, and the change in kink angle $\Delta\varphi$, see Fig. A3(b),

$$\varphi_2 = \varphi_1 + \Delta\varphi. \tag{A13}$$

If the second step is considered, the fibre will expand in the transverse direction only if the moisture is increased. If the fibre is curved, or have a kink, the fibre can not just expand in the transverse direction because of geometrical reasons. As shown in Fig. A3(a) half the fibre has expanded in that way and it can be seen that the compatibility is not satisfied. Instead the fibre has to straighten up, as shown in Fig. A3(b), i.e. $\varphi_2 < \varphi_1$ and the change $\Delta\varphi < 0$.

To determine the change in the kink angle, $\Delta\varphi$, caused by the expansion in the transverse direction, $\Delta\varepsilon_T^2$, an enlargement of Fig. A3(a) is analysed, as shown in Fig. A4, i.e. half the fibre is considered and the geometrical effect of the other half is disregarded. The deformations shown in Figs. A3 and A4 are exaggerated. If small deformations are assumed the change is approximately

$$\Delta\varphi = -\Delta\varepsilon_T^2\varphi_1. \tag{A14}$$

The kink angle, θ, is twice the angle φ. If Eq. (A9) is used the change in kink angle, $\Delta\theta$, can be expressed as

$$\Delta\theta = 2\Delta\varphi = -(\beta_T - \beta_L)\theta_1\Delta m, \tag{A15}$$

where the angle θ_1 is the sum of the initial angle θ_0 and the creep angle θ_c, cf. Eq. (A12). The hygroexpansion coefficient for the kink angle β_m is defined as

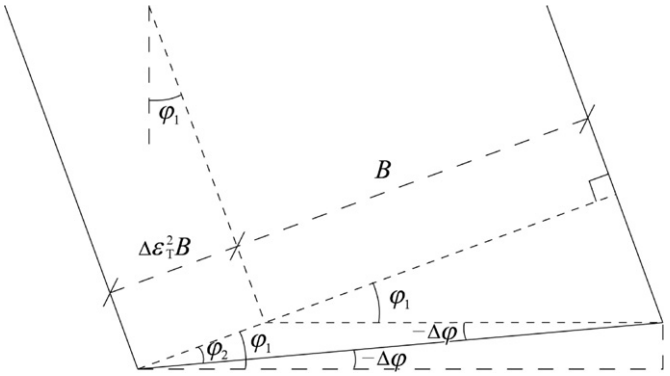

Fig. A4. Enlargement of the area close to the kink in the left figure in Fig. A3.

$$\beta_m = \frac{\Delta\theta}{\Delta m}. \tag{A16}$$

Eqs. (A15) and (A16) gives an estimation of the hygroexpansion coefficient for the kink angle

$$\beta_m = -(\beta_T - \beta_L)\cdot(\theta_0 + \theta_c). \tag{A17}$$

Since $\beta_T > \beta_L$ the hygroexpansion coefficient for the kink angle β_m becomes negative, which is reasonable since an increase in moisture should straighten out the fibre, i.e. give a negative change in kink angle, $\Delta\theta < 0$.

A.3. Estimation of the material parameters in the creep law for the spring, K_1, K_2, K_3

Here it is assumed that the deformation in the fibres is caused by creep only, i.e. the kink angle θ, see Fig. A1, consist partly of the initial angle θ_0, and partly of the creep angle θ_c,

$$\theta = \theta_0 + \Delta\theta = \theta_0 + \theta_c. \tag{A18}$$

The elastic and hygroexpansive deformations are neglected. It is assumed that the angle change caused by creep in the spring is given by the creep law

$$\dot{\theta}_c = K_1 \sinh(K_2(M - K_3\theta_c)), \tag{A19}$$

where M is the torsional spring moment and K_1, K_2, K_3 are material parameters that should be estimated.

To estimate the material parameters the fibre model shown in Fig. A1 is approximated with beams, in the same way as in Appendix A1, see Figs. A2 and A5. The beams are bent and the creep in the beams is assumed to be given by the same law as the creep in the bars, i.e.

$$\dot{\varepsilon}_c = a \sinh(b(\sigma - E_c\varepsilon_c)), \tag{A20}$$

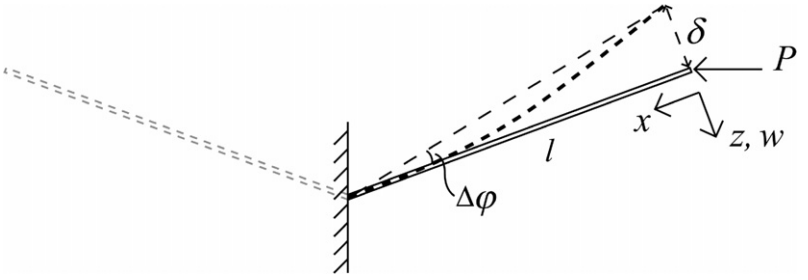

Fig. A5. The fibre model is approximated with two rigidly clamped beams so that a beam model can be used to estimate the material parameters in the creep law for the spring.

where σ is the stress in the fibre, a, b and E_c are considered to be known material constant. This creep also gives a change in the curvature. Below, an order-of-magnitude estimation will be presented. From beam bending theory, the strain is given by

$$\varepsilon_c = \varepsilon = -z\kappa, \tag{A21}$$

where, z is the coordinate transverse to the beam and $\kappa = 1/R$ is the curvature of the beam. The curvature depends on the angle $\Delta\varphi$,

$$\kappa \approx \frac{2\Delta\varphi}{l}, \tag{A22}$$

where l is the length of the beam. If Eq. (A22) is inserted into Eq. (A21) the strain can be approximated as

$$\varepsilon_c \approx \frac{\theta_c H}{l} f_1, \tag{A23}$$

where H is the height of the beam and f_1 is a non-dimensional function. The stress in the beam can be approximated as

$$\sigma \approx \frac{MH}{I} f_2 \approx \frac{M}{BH^2} f_2, \tag{A24}$$

where B is the width of the beam and f_2 is another non-dimensional function. Eqs. (A23) and (A24) are inserted into Eq. (A20), and solving for $\dot{\theta}_c$ gives

$$\dot{\theta}_c \approx \frac{al}{H} \cdot \frac{1}{f_1} \left[\frac{b}{BH^2} f_2 \left(M - \frac{E_c BH^3}{l} \cdot \frac{f_1}{f_2} \theta_c \right) \right]. \tag{A25}$$

By comparing Eqs. (A19) and (A25) a reasonable estimation of the material parameters K_1, K_2 and K_3 in the creep law for the spring can be obtained as,

$$K_1 = k_1 \frac{al}{H}, \tag{A26}$$

$$K_2 = k_2 \frac{b}{BH^2}, \tag{A27}$$

$$K_3 = k_3 \frac{E_c BH^3}{l}, \tag{A28}$$

where k_1, k_2, k_3 are non-dimensional constants.

A.4. Numerical solution to the network problem

Vector notation is introduced after the discretisation, this will simplify the solution step, especially because most of the equations that control the network are linear equations. The fibre angles, which are known and given by Eq. (35), can be expressed in vector notation as a $N \times 1$ vector,

$$\boldsymbol{\alpha} = \begin{bmatrix} 0 & \frac{\pi}{N} & \frac{2\pi}{N} & \cdots & \frac{(N-1)\pi}{N} \end{bmatrix}^{\mathrm{T}}. \tag{A29}$$

The variables that depend on the fibre angle α are also expressed in vector notation, for example the average strain of the fibres can be expressed as

$$\boldsymbol{\varepsilon} = [\, \varepsilon_1 \quad \varepsilon_2 \quad \cdots \quad \varepsilon_N \,]^{\mathrm{T}}. \tag{A30}$$

In the same way can the strains and stresses in the different fibre sections, $\boldsymbol{\varepsilon}_A, \boldsymbol{\varepsilon}_B, \boldsymbol{\varepsilon}_C, \boldsymbol{\varepsilon}_A^c, \boldsymbol{\varepsilon}_B^c, \boldsymbol{\varepsilon}_C^c, \boldsymbol{\sigma}_A, \boldsymbol{\sigma}_B, \boldsymbol{\sigma}_C$, be expressed in vector notation, i.e. as $N \times 1$ vectors. The kink angle $\boldsymbol{\theta}$, the kink angle change caused by creep $\boldsymbol{\theta}_c$ and the initial kink angle $\boldsymbol{\theta}_0$ are also expressed as $N \times 1$ vectors. Here the initial kink angle, θ_0, is considered to be known and is also assumed to be the same for all fibres and all fibre segments, i.e.

$$\boldsymbol{\theta_0} = [\,\theta_0 \quad \theta_0 \quad \cdots \quad \theta_0\,]^{\mathrm{T}} = \theta_0 \mathbf{E}, \tag{A31}$$

where $\mathbf{E}$ is a $N \times 1$ vector with ones, i.e.

$$\mathbf{E} = [\,1 \quad 1 \quad 1 \quad \cdots\,]^{\mathrm{T}}. \tag{A32}$$

The macroscopic stresses and strains are also expressed in vector notation, i.e.

$$\bar{\boldsymbol{\varepsilon}} = [\,\bar{\varepsilon}_1 \quad \bar{\varepsilon}_2 \quad \bar{\gamma}_{12}\,]^{\mathrm{T}}, \tag{A33}$$

$$\bar{\boldsymbol{\sigma}} = [\,\bar{\sigma}_1^{\mathrm{w}} \quad \bar{\sigma}_2^{\mathrm{w}} \quad \bar{\tau}_{12}^{\mathrm{w}}\,]^{\mathrm{T}}. \tag{A34}$$

The equations that control the network are given by the linear Eqs. (19)–(25), (27), (28) and the non-linear Eqs. (29), (33). Eqs. (20)–(22), (27), (28) expressed in vector notation become

$$\boldsymbol{\varepsilon} = \lambda \boldsymbol{\varepsilon}_{\mathbf{A}} + (1-\lambda)\boldsymbol{\varepsilon}_{\mathbf{B}}, \tag{A35}$$

$$\boldsymbol{\varepsilon}_{\mathbf{C}} = \boldsymbol{\varepsilon}_{\mathbf{B}}, \tag{A36}$$

$$\boldsymbol{\sigma}_{\mathbf{A}} = \boldsymbol{\sigma}_{\mathbf{B}} + \boldsymbol{\sigma}_{\mathbf{C}}, \tag{A37}$$

$$\boldsymbol{\varepsilon}_{\mathbf{B}} = \frac{\boldsymbol{\sigma}_{\mathbf{B}}}{E_{\mathrm{L}}} + \boldsymbol{\varepsilon}_{\mathbf{B}}^{\mathbf{c}} + \beta_{\mathrm{L}} \Delta m \mathbf{E}, \tag{A38}$$

and

$$\boldsymbol{\varepsilon}_{\mathbf{C}} = \frac{\boldsymbol{\sigma}_{\mathbf{C}}}{E_{\mathrm{T}}} + \boldsymbol{\varepsilon}_{\mathbf{C}}^{\mathbf{c}} + \beta_{\mathrm{T}} \Delta m \mathbf{E}. \tag{A39}$$

The linear Eq. (19) can be expressed as

$$\boldsymbol{\varepsilon} = \boldsymbol{\Psi} \bar{\boldsymbol{\varepsilon}}, \tag{A40}$$

where $\boldsymbol{\Psi}$ is a $N \times 3$ matrix dependent on the fibre angles,

$$\boldsymbol{\Psi} = \begin{bmatrix} \cos^2\alpha_1 & \sin^2\alpha_1 & \cos\alpha_1 \sin\alpha_1 \\ \cos^2\alpha_2 & \sin^2\alpha_2 & \cos\alpha_2 \sin\alpha_2 \\ \vdots & \vdots & \vdots \\ \cos^2\alpha_N & \sin^2\alpha_N & \cos\alpha_N \sin\alpha_N \end{bmatrix}. \tag{A41}$$

The linear Eqs. (23)–(25) can be expressed as

$$\bar{\boldsymbol{\sigma}} = \mathbf{q} \boldsymbol{\sigma}_{\mathbf{A}}, \tag{A42}$$

where $\mathbf{q}$ is a $3 \times N$ matrix dependent on the fibre angles, the number of fibres and the fibre density,

$$\mathbf{q} = \frac{1}{N\rho_f} \begin{bmatrix} \cos^2\alpha_1 & \cos^2\alpha_2 & \cdots & \cos^2\alpha_N \\ \sin^2\alpha_1 & \sin^2\alpha_2 & \cdots & \sin^2\alpha_N \\ \cos\alpha_1 \sin\alpha_1 & \cos\alpha_2 \sin\alpha_2 & \cdots & \cos\alpha_N \sin\alpha_N \end{bmatrix}. \tag{A43}$$

The frequency function $f(\alpha) = 1/\pi$ has been used. The non-linear Eqs. (29) and (33) expressed in vector notation become

$$\boldsymbol{\varepsilon}_{\mathbf{A}} = \frac{\boldsymbol{\sigma}_{\mathbf{A}}}{E_{\mathrm{L}}} + \beta_{\mathrm{L}} \Delta m \mathbf{E} + \boldsymbol{\varepsilon}_{\mathbf{A}}^{\mathbf{c}} + \frac{1}{8}\left(\theta_0^2 \mathbf{E} - \boldsymbol{\theta}_{\mathbf{sq}}\right), \tag{A44}$$

$$\boldsymbol{\theta} = \theta_0 \mathbf{E} + \boldsymbol{\theta}_{\mathbf{c}} - \frac{Al^2}{2q_{\mathrm{k}} E_{\mathrm{L}} I} \mathbf{D} - (\beta_{\mathrm{T}} - \beta_{\mathrm{L}}) \cdot (\theta_0 \mathbf{E} + \boldsymbol{\theta}_{\mathbf{c}}) \Delta m, \tag{A45}$$

where the vectors $\boldsymbol{\theta}_{\mathbf{sq}}$ and $\mathbf{D}$ are defined as

$$\boldsymbol{\theta}_{\mathbf{sq}} = [\,\theta_1^2 \quad \theta_2^2 \quad \cdots \quad \theta_N^2\,]^{\mathrm{T}} \tag{A46}$$

and

$$\mathbf{D} = [\,\sigma_{A1}\theta_1 \quad \sigma_{A2}\theta_2 \quad \cdots \quad \sigma_{AN}\theta_N\,]^T. \tag{A47}$$

Eqs. (A35)–(A40), (A44), (A45), define $8N$ equations and Eq. (A42) defines three more equations. The creep laws, Eqs. (30)–(32), (34), which give the creep strains in the different sections and also the creep part of the kink angle, is valid for each fibre, for example $\dot{\varepsilon}^c_{A1} = a_L \sinh\left(b_L\left(\sigma_{A1} - E^c_L \varepsilon^c_{A1}\right)\right)$. This gives $4N$ additional equations. Now all equations that control the network are known. If, for example, the macroscopic specific stresses in the paper $\bar{\boldsymbol{\sigma}}$ together with the moisture variations Δm are known, then the macroscopic strains of the paper $\bar{\boldsymbol{\varepsilon}}$ and all internal variables can be determined.

If $\bar{\boldsymbol{\sigma}}$ is prescribed, Eqs. (A35)–(A40), (A42) can be used to express $\bar{\boldsymbol{\varepsilon}}$ as

$$\bar{\boldsymbol{\varepsilon}} = \frac{1-\lambda}{E_L + E_T}\mathbf{S}\bar{\boldsymbol{\sigma}} + \lambda \mathbf{S}\mathbf{q}\boldsymbol{\varepsilon}_A + \frac{E_L(1-\lambda)}{E_L+E_T}\mathbf{S}\mathbf{q}\left(\boldsymbol{\varepsilon}^c_B + \beta_L \Delta m \mathbf{E}\right) + \frac{E_T(1-\lambda)}{E_L+E_T}\mathbf{S}\mathbf{q}\left(\boldsymbol{\varepsilon}^c_C + \beta_T \Delta m \mathbf{E}\right), \tag{A48}$$

where

$$\mathbf{S} = [\mathbf{q}\boldsymbol{\Psi}]^{-1}. \tag{A49}$$

Solving Eqs. (A35)–(A40), (A42), (A44) for the stress $\boldsymbol{\sigma}_A$ leads to the following equation:

$$\boldsymbol{\sigma}_A = \mathbf{Q}\left(\mathbf{I} - \frac{1}{E_L}\mathbf{Q}\right)^{-1}\left[\frac{1}{E_L}\mathbf{R} + \boldsymbol{\varepsilon}^c_A + \beta_L \Delta m \mathbf{E} + \frac{1}{8}\left(\theta_0^2 \mathbf{E} - \boldsymbol{\theta}_{sq}\right)\right] + \mathbf{R}, \tag{A50}$$

where

$$\mathbf{Q} = (E_L + E_T)\frac{\lambda}{1-\lambda}(\boldsymbol{\Psi}\mathbf{S}\mathbf{q} - \mathbf{I}) \tag{A51}$$

and

$$\mathbf{R} = \boldsymbol{\Psi}\mathbf{S}\bar{\boldsymbol{\sigma}} + (\boldsymbol{\Psi}\mathbf{S}\mathbf{q} - \mathbf{I})\left[E_L\left(\boldsymbol{\varepsilon}^c_B + \beta_L \Delta m \mathbf{E}\right) + E_T\left(\boldsymbol{\varepsilon}^c_C + \beta_T \Delta m \mathbf{E}\right)\right]. \tag{A52}$$

The stresses in the other parts of the fibres, $\boldsymbol{\sigma}_B$ and $\boldsymbol{\sigma}_C$, can be expressed in $\boldsymbol{\sigma}_A$ by using Eqs. (A36)–(A39),

$$\boldsymbol{\sigma}_B = \frac{1}{1/E_L + 1/E_T}\left[\frac{1}{E_T}\boldsymbol{\sigma}_A + \boldsymbol{\varepsilon}^c_C - \boldsymbol{\varepsilon}^c_B + (\beta_T - \beta_L)\Delta m \mathbf{E}\right], \tag{A53}$$

$$\boldsymbol{\sigma}_C = \frac{1}{1/E_L + 1/E_T}\left[\frac{1}{E_L}\boldsymbol{\sigma}_A + \boldsymbol{\varepsilon}^c_B - \boldsymbol{\varepsilon}^c_C + (\beta_L - \beta_T)\Delta m \mathbf{E}\right]. \tag{A54}$$

The stresses according to Eqs. (A50)–(A54) are substituted into the creep laws, Eqs. (30)–(32), (34) and into the non-linear equation for the kink angle, Eq. (A45). Then the Eqs. (30)–(32), (34) define a system of first order ordinary differential equations that must be solved simultaneously as the non-linear equation for the kink angle, $\boldsymbol{\theta}$, Eq. (A45). The initial conditions for all creep strains and for the creep part of the kink angle is that they are zero. When the system of equations has been solved the strains $\boldsymbol{\varepsilon}^c_A, \boldsymbol{\varepsilon}^c_B, \boldsymbol{\varepsilon}^c_C$ and the angles $\boldsymbol{\theta}_c$, $\boldsymbol{\theta}$ are known. The stresses in the different parts of the fibres, $\boldsymbol{\sigma}_A$, $\boldsymbol{\sigma}_B$ and $\boldsymbol{\sigma}_C$, can then be calculated using Eqs. (A50)–(A54). After that, the strains in the different parts of the fibres, $\boldsymbol{\varepsilon}_A$, $\boldsymbol{\varepsilon}_B$ and $\boldsymbol{\varepsilon}_C$, can be determined using Eqs. (A38), (A39), (A44). Finally, the macroscopic strain $\bar{\boldsymbol{\varepsilon}}$ can be calculated by using Eq. (A48). The introduced variables and constants K_1, K_2, K_3, $\mathbf{E}$, $\boldsymbol{\Psi}$, $\mathbf{q}$, $\mathbf{S}$, $\mathbf{Q}$ and $\mathbf{R}$ are given by Eqs. (16)–(18), (A32), (A41), (A43), (A49), (A51) and (A52), respectively.

If macroscopic strains are prescribed instead of stresses it is possible to obtain the macroscopic stresses in a similar way as described above. The same system of equations are obtained, the only difference is $\mathbf{Q}$ and $\mathbf{R}$, which changes to

$$\mathbf{Q} = -\frac{\lambda}{1-\lambda}(E_L + E_T)\mathbf{I}, \tag{A55}$$

$$\mathbf{R} = \frac{(E_L + E_T)}{1-\lambda}\boldsymbol{\Psi}\bar{\boldsymbol{\varepsilon}} - \left[E_L\left(\boldsymbol{\varepsilon}^c_B + \beta_L \Delta m \mathbf{E}\right) + E_T\left(\boldsymbol{\varepsilon}^c_C + \beta_T \Delta m \mathbf{E}\right)\right]. \tag{A56}$$

References

Alfthan, J., Gudmundson, P., Östlund, S., 2002. A micro-mechanical model for mechano-sorptive creep in paper. Journal of Pulp and Paper Science 28 (3), 98–104.

Alfthan, J., 2003. A simplified network model for mechano-sorptive creep in paper. Journal of Pulp and Paper Science 29 (7), 228–234.

Alfthan, J., 2004. The effect of humidity cycle amplitude on accelerated tensile creep of paper. Mechanics of Time-Dependent Materials 8 (4), 289–302.

Alfthan, J., Gudmundson, P., 2005. Linear constitutive model for mechano-sorptive creep in paper. International Journal of Solids and Structures 42 (24–25), 6261–6276.

Armstrong, L.D., Kingston, R.S.T., 1960. Effect of moisture changes on creep in wood. Nature 185 (4716), 862–863.

Armstrong, L.D., Christensen, G.N., 1961. Influence of moisture changes on deformation of wood under stress. Nature 191 (4791), 869–870.

Bergander, A., Salmén, L., 2002. Cell wall properties and their effects on the mechanical properties of fibers. Journal of Materials Science 37 (1), 151–156.

Brezinski, J.P., 1956. The creep properties of paper. Tappi 39 (2), 116–128.

Byrd, V.L., 1972a. Effect of relative humidity changes during creep on handsheet paper properties. Tappi 55 (2), 247–252.

Byrd, V.L., 1972b. Effect of relative humidity changes on compressive creep response of paper. Tappi 55 (11), 1612–1613.

Cox, H.L., 1952. The elasticity and strength of paper and other fibrous materials. British Journal of Applied Physics 3 (3), 72–79.

DeMaio, A., Patterson, T., 2006. Influence of bonding on the tensile creep behavior of paper in a cyclic humidity environment. Mechanics of Time-Dependent Materials 10 (1), 17–33.

Gallay, W., 1973. Stability of dimensions and form of paper. Tappi 56 (11), 54–63.

Gellerstedt, G. (Ed.), 2004. The Ljungberg Textbook, Paper Physics. KTH Fibre and Polymer Technology, Royal Institute of Technology (KTH), Stockholm, Sweden, Chapter 47, p. 12.

Gibson, E.J., 1965. Creep of wood: Role of water and effect of a changing moisture content. Nature 206 (4980), 213–215.

Gunderson, D.E., Tobey, W.E., 1990. Tensile creep of paperboard – effect of humidity change rates. In: Caulfield, D.F., Passaretti, J.D., Sobczynski, S.F. (Eds.), Materials interaction relevant to the pulp, paper, and wood industries. Materials Research Society symposium proceedings, vol. 197, San Francisco, California, pp. 213–226.

Habeger, C.C., Coffin, D.W., 2000. The role of stress concentrations in accelerated creep and sorption-induced physical aging. Journal of Pulp and Paper Science 26 (4), 145–157.

Halsey, G., White, H.J., Eyring, H., 1945. Mechanical properties of textiles, I. Textile Research Journal 15 (9), 295–311.

Haslach, H.W., 1994. The mechanics of moisture accelerated tensile creep in paper. Tappi Journal 77 (10), 179–186.

Haslach, H.W., Zeng, N., 1999. Maximum dissipation evolution equations for non-linear thermoviscoelasticity. International Journal of Non-linear Mechanics 34 (2), 361–385.

Hoffmeyer, P., Davidson, R.W., 1989. Mechano-sorptive creep mechanism of wood in compression and bending. Wood Science and Technology 23 (3), 215–227.

Hoffmeyer, P., 1993. Non-linear creep caused by slip plane formation. Wood Science and Technology 27 (5), 321–335.

Holland, H.D., Halsey, G., Eyring, H., 1946. Mechanical properties of textiles, VI A study of creep of fibers. Textile Research Journal 16 (5), 201–210.

Karlsson, H., Fransson, P.-I., 1994. STFI FiberMaster gives papermakers new muscle – new knowledge concerning fiber shape can be the key to paper of the future. Svensk Papperstidning Nordisk Cellulosa 97 (10), 26–28.

Komori, T., Makishima, K., 1977. Numbers of fiber-to-fiber contacts in general fiber assemblies. Textile Research Journal 47 (1), 13–17.

Mackay, B.H., Downes, J.G., 1959. The effect of the sorption process on the dynamic rigidity modulus of the wool fiber. Journal of Applied Polymer Science 2 (4), 32–38.

MATLAB, 2006. MATLAB 7.3.0. The MathWorks, Inc, Natick, Massachusetts.

Mohlin, U.-B., Dahlbom, J., Hornatowska, J., 1996. Fiber deformation and sheet strength. Tappi Journal 79 (6), 106–111.

Mårtensson, A., 1994. Mechano-sorptive effects in wooden material. Wood Science and Technology 28 (6), 437–449.

Neagu, R.C., 2006. Hygroelastic behaviour of wood-fibre based materials on the composite, fibre and ultrastructural level. PhD Thesis, KTH Solid Mechanics, Royal Institute of Technology (KTH), Stockholm, Sweden, pp. D20 and F9.

Niskanen, K. (Ed.), 1998. Paper Physics, Papermaking Science and Technology book 16. Fapet Oy, Helsinki, pp. 57, 59, 91 and 233.

Nordon, P., 1962. Some torsional properties of wool fibers. Textile Research Journal 32 (7), 560–568.

Olsson, A.-M., Salmén, L., 2001. Molecular mechanisms involved in creep phenomena of paper. Journal of Applied Polymer Science 79 (9), 1590–1595.

Olsson, A.-M., Salmén, L., Eder, M., Burgert, I., 2007. Mechano-sorptive creep in wood fibres. Wood Science and Technology 41 (1), 59–67.

Padanyi, Z.V., 1991. Mechano-sorptive effects and accelerated creep in paper. In: 1991 International Paper Physics Conference Proceedings, Kona, Hawaii, pp. 397–411.

Padanyi, Z.V., 1993. Physical aging and glass transition: Effects on the mechanical properties of paper and board. In: Baker, C.F. (Ed.), Products of Papermaking, Transactions of the Tenth Fundamental Research Symposium Held at Oxford, vol. 1. Pira International, Leatherhead, pp. 521–545.

Page, D.H., Tydeman, P.A., 1962. A new theory of the shrinkage, structure and properties of paper. In: Bolam, F. (Ed.), The Formation and Structure of Paper, Transactions of the Symposium Held at Oxford September 1961. British Paper and Board Makers Association, Technical Section, London, pp. 397–425.

Panek, J., Fellers, C., Haraldsson, T., 2004. Principles of evaluation for the creep of paperboard in constant and cyclic humidity. Nordic Pulp & Paper Research Journal 19 (2), 155–163.

Pickett, G., 1942. The effect of change in moisture-content of the creep of concrete under a sustained load. Journal of the American Concrete Institute 13 (4), 333–355.

Ranta-Maunus, A., 1975. The viscoelasticity of wood at varying moisture content. Wood Science and Technology 9 (3), 189–205.

Salmén, L., 2004. Micromechanical understanding of the cell-wall structure. Comptes Rendus Biologies 327 (9–10), 873–880.

Schulgasser, K., Page, D.H., 1988. The influence of transverse fibre properties on the in-plane elastic behaviour of paper. Composites Science and Technology 32 (4), 279–292.

Sedlachek, K.M., 1995. The effect of hemicelluloses and cyclic humidity on the creep of single fibers. PhD Thesis, Institute of Paper Science and Technology, Atlanta, Georgia.

Söremark, C., Fellers, C., 1993. Mechano-sorptive creep and hygroexpansion of corrugated board in bending. Journal of Pulp and Paper Science 19 (1), J19–J26.

Söremark, C., Fellers, C., Henriksson, L., 1993. Mechano-sorptive creep of paper – Influence of drying restraint and fibre orientation. In: Baker, C.F. (Ed.), Products of Papermaking, Transactions of the Tenth Fundamental Research Symposium Held at Oxford, vol. 1. Pira International, Leatherhead, pp. 547–574.

Urbanik, T.J., 1995. Hygroexpansion-creep model for corrugated fiberboard. Wood and Fiber Science 27 (2), 134–140.

van den Akker, J.A., 1962. Some theoretical considerations on the mechanical properties of fibrous structures. In: Bolam, F. (Ed.), The Formation and Structure of Paper, Transactions of the Symposium Held at Oxford September 1961, vol. 1. British Paper and Board Makers Association, Technical Section, London, pp. 205–241.

Wang, J.Z., Dillard, D.A., Wolcott, M.P., Kamke, F.A., Wilkes, G.L., 1990. Transient moisture effect in fibers and composite materials. Journal of Composite Materials 24 (9), 994–1009.

Wang, J.Z., Dillard, D.A., Ward, T.C., 1992. Temperature and stress effects in the creep of aramid fibers under transient moisture conditions and discussions on the mechanism. Journal of Polymer Science Part B: Polymer Physics 30 (12), 1391–1400.

Wang, J.Z., Davé, V., Glasser, W., Dillard, D.A., 1993. The effects of moisture sorption on the creep behavior of fibers. In: Harris, C., Gates, T. (Eds.), High Temperature and Environmental Effects on Polymeric Composites, ASTM STP 1174. American Society for Testing and Materials, Philadelphia, pp. 186–200.